Acta Pharmaceutica Sinica B 2026;16(3):1625−1642

Chinese Pharmaceutical Association
Institute of Materia Medica, Chinese Academy of Medical Sciences

Acta Pharmaceutica Sinica B

www.elsevier.com/locate/apsb
www.sciencedirect.com

ORIGINAL ARTICLE

Liposomal simvastatin potentiates intranasal H1N1 influenza subunit vaccine *via* increasing transcytosis of antigen and submucosal dendritic cell recruitment

Afeng Yang[a], Chen Zhang[a], Aihua Wu[a], Jiaojiao Xu[a], Hongzheng Lin[a], Zhe Li[a], Tingting Li[a], Yunlu Li[a], Ningshao Xia[b], Xunlong Shi[a,*], Tianying Zhang[b,*], Wei Lu[a,*]

[a]*School of Pharmaceutical Sciences, Minhang Hospital, Key Laboratory of Smart Drug Delivery Ministry of Education & State Key Laboratory of Molecular Engineering of Polymers, Fudan University, Shanghai 201203, China*
[b]*State Key Laboratory of Vaccines for Infectious Diseases, Xiang An Biomedicine Laboratory, School of Public Health, Xiamen University, Xiamen 361102, China*

Received 26 June 2025; received in revised form 29 October 2025; accepted 20 November 2025

KEY WORDS

Intranasal adjuvant;
Liposomes;
Simvastatin;
Subunit vaccine;
H1N1 influenza;
Transcytosis of antigens;
Nasal epithelial cells;
Dendritic cell recruitment

Abstract Intranasal vaccines specifically eliciting mucosal immunity in the upper respiratory tract have shown advantages in protecting against respiratory virus invasion. Yet, no clinically licensed intranasal adjuvant remains a major hurdle for the development of intranasal vaccines with low immunogenic antigens like subunit vaccines. Here, we show that liposomes loading simvastatin (Lipo-SV) serve as potent mucosal adjuvants for the intranasal liposomal subunit vaccine encapsulating the hemagglutinin 1 (HA1) glycoprotein of A/PR/8/34 (PR8) H1N1 influenza (Lipo-HA1), providing robust protection against the lethal PR8 H1N1 infection. Compared to cholera toxin subunit B (CTB), the only mucosal adjuvant used in humans, the Lipo-SV substantiate intranasal Lipo-HA1 vaccines to elicit robust systemic and local mucosal immune responses. The underlying mechanism of the adjuvanticity of Lipo-SV involves the increased transcytosis of antigens by inhibiting the geranylgeranylation of RAB5 and RAB7B GTPases in nasal epithelial cells. Moreover, Lipo-SV enhance the submucosal recruitment of dendritic cell for antigen uptake *via* the Toll-like receptor 4-dependent pathway. Unlike CTB, intranasal Lipo-SV do not

*Corresponding authors.
E-mail addresses: xunlongshi@fudan.edu.cn (Xunlong Shi), zhangtianying@xmu.edu.cn (Tianying Zhang), wlu@fudan.edu.cn (Wei Lu).

Peer review under the responsibility of Chinese Pharmaceutical Association and Institute of Materia Medica, Chinese Academy of Medical Sciences.

https://doi.org/10.1016/j.apsb.2025.12.021

induce inflammation in the lung or the inflammatory cytokines in the central nervous system. Our results present a paradigm of design of mucosal adjuvant to target the mucosal epithelial cells in addition to the antigen-presenting cells.

1. Introduction

The respiratory mucosal immune system serves as the first line of physical and immunological defense against invasion of respiratory viral pathogens. Although the vaccines through intramuscular (i.m.) administration induce serum immunoglobulin G (IgG) against infectious diseases, they are unable to induce efficient mucosal immunity[1]. Vaccination *via* the nasal route represents an appealing strategy for inducing both antigen-specific systemic and mucosal immunity. Compared to intramuscular vaccines, intranasal vaccines can elicit secretory IgA (SIgA) in the nasal passages and upper airways as well as tissue-resident memory cells (TRMs) in the lungs to prevent early invasion of pathogens in the respiratory tract, which is desirable[2–4].

The currently intranasal vaccines for human use against respiratory viral pathogens are primarily live attenuated or inactivated vaccines[5]. Subunit vaccines, using pathogen-derived proteins or peptides as vaccine antigens, have advantages over live attenuated vaccines or inactivated vaccines in terms of safety and production costs[6]. However, the efficacy of intranasal subunit vaccines is compromised due to the physiologic barriers of the nasal cavity, such as the epithelial layer, ciliary clearance, mucus layer, and degradation by the secreted lysozymes[7]. These barriers restrict a sufficient amount of antigen from being delivered to the submucosal lamina propria, where dendritic cells (DCs) can capture the antigen and mature[8]. With the development of bioengineering and material sciences, various nanoparticulate vaccine delivery systems have been designed to overcome the mucosal barriers to improve the nasal antigen delivery, such as liposomes, polymers, hydrogels, chitosan, etc.[9,10]. Among them, liposomal formulations are widely used in various human vaccines[11]. Intranasal (i.n.) administration of liposomes loading *Streptococcus mutans* antigen can induce significantly higher IgA titers than the free antigen in healthy adults[12]. Besides, liposomal formulations are clinically used as adjuvant delivery systems, such as AS01[13].

Besides the vaccine delivery systems, successful intranasal subunit vaccines rely on adjuvants that can induce robust and durable immune responses[14,15]. Existing adjuvants licensed in human vaccines are mostly for injectable vaccines[16,17]. Among these adjuvants, aluminum salts induce Th2 immune responses through depot effect, while others like AS01 and CpG elicit cellular immunity through triggering multiple signaling pathways of host pattern recognition receptors (PRRs)[18,19]. Nowadays, the exploration of adjuvants primarily focuses on the molecules targeting antigen-presenting cells (APCs) to activate innate immune signals, such as Toll-like receptor (TLR) agonists, stimulator of interferon genes (STING) agonists, and immune-stimulating complexes (ISCOMs)[18]. Yet, these adjuvants have not been licensed for use in mucosal vaccines.

Cholera toxins (CT) have been well-studied and regarded as one of the most potent mucosal adjuvants, consisting of a monomeric "A" (CTA) and a pentameric "B" subunit (CTB)[20]. Its B subunit binds to gangliosides, preferentially GM1 on epithelial cell membranes, to enhance antigen transport across the epithelium. However, CTA for human use has been constrained due to local or systemic toxicity, such as overt diarrhea[21]. CTB is nontoxic and added to the oral cholera vaccine, which is the only licensed non-living mucosal vaccine available for human use[5]. CTB can assist an intranasal vaccine in inducing robust systemic and mucosal immune responses in animal models[22]. However, CTB is highly immunogenic and potentially neurotoxic due to its capacity to bind to gangliosides presented on all nucleated cells[5]. Therefore, there is an urgent need to develop effective and safe mucosal adjuvants for intranasal subunit vaccines.

We hypothesize that adjuvants targeting nasal epithelial cells (ECs) to facilitate the transmucosal delivery of antigen and submucosal antigen uptake could potentiate intranasal subunit vaccines against respiratory viruses. Simvastatin (SV) has been reported to activate DCs as a vaccine adjuvant through arrested endosomal maturation and increased antigen presentation by inhibiting the geranylgeranylation of RAB5 guanosine triphosphatase (GTPases)[23,24]. However, the ability of SV as mucosal adjuvant remains unknown. Herein, we prepare liposomes loading SV (Lipo-SV) serving as mucosal adjuvant for intranasal vaccines. Intranasal immunization with Lipo-SV significantly promotes systemic or mucosal immunity induced by intranasal liposomal subunit vaccines encapsulating the hemagglutinin 1 (HA1) glycoprotein of the A/PR/8/34 (PR8) H1N1 influenza (Lipo-HA1) or the receptor-binding domain (RBD) of the spike protein of SARS-CoV-2 prototype (Lipo-RBD), with high levels of IgG1, IgG or IgA, cytotoxic T lymphocytes (CTLs) and $CD8^+$ TRMs responses. The mice intranasally immunized with Lipo-SV plus Lipo-HA1 vaccines establish a formidable defense against the lethal PR8 H1N1 influenza virus. Lipo-SV inhibit the formation of geranylgeranyl diphosphate (GGPP), a metabolite downstream of the mevalonate (MVA) pathway, which is required for geranylgeranylation of RAB5 and RAB7B GTPases in the nasal ECs. The decreased amount of RAB5 localized on cell membranes increases the transcytosis of the subunit vaccine by reducing the transport of antigens from early endosomes to lysosomes. Meanwhile, Lipo-SV increase the number of $TLR4^+$ ECs as a result of reduced expression of RAB7B in EC membranes. This leads to submucosal recruitment of dendritic cells for antigen uptake *via* enhanced expression of C-C motif chemokine ligand (CCL) 20. Consequently, the antigen-loaded DCs quickly migrate into cervical lymph nodes (CLNs) for antigen presentation (Fig. 1). Our results demonstrate the mechanism of adjuvanticity of Lipo-SV for intranasal H1N1 influenza vaccines, and the nasal epithelium being a promising target for mucosal adjuvants.

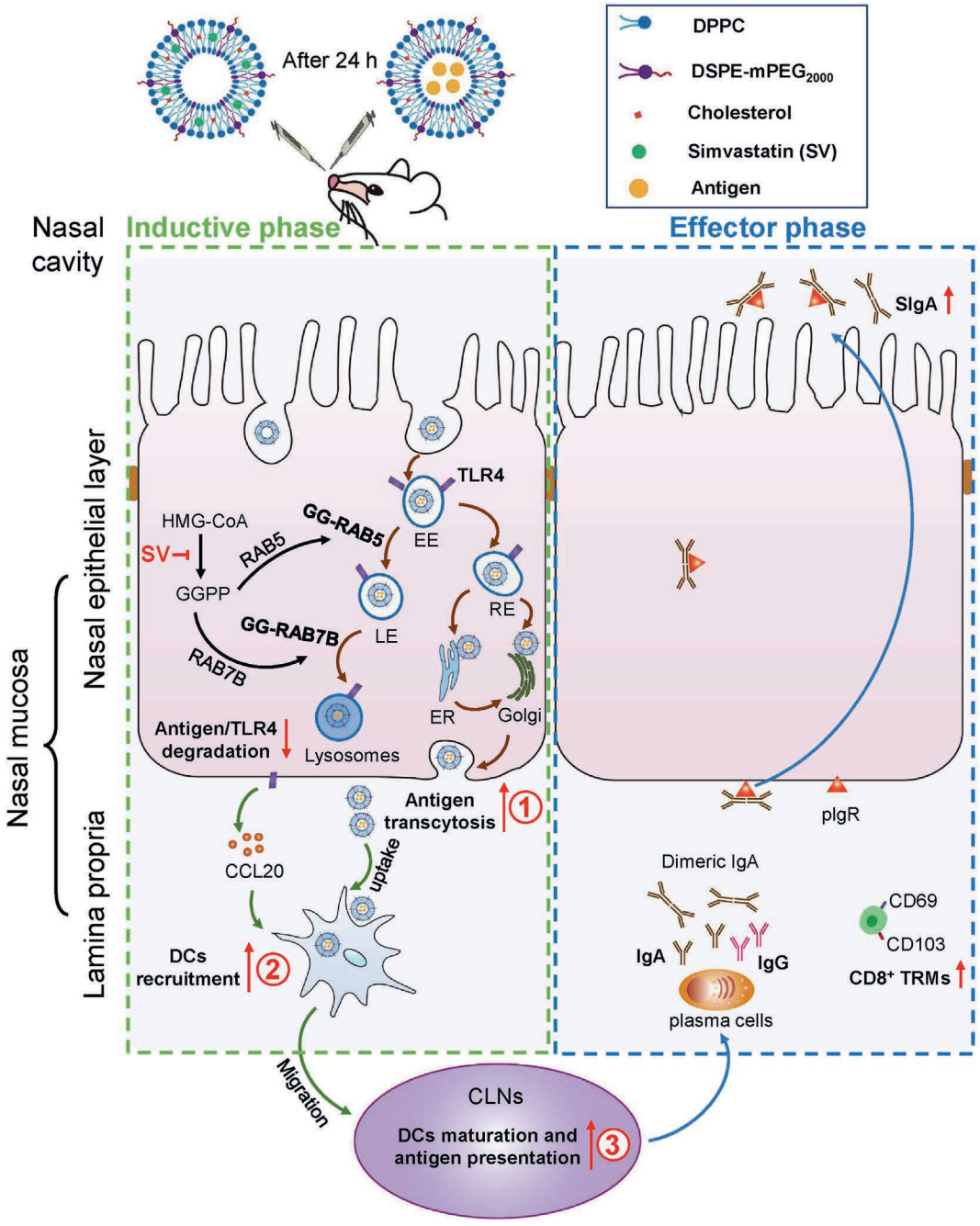

Figure 1 Schematic illustration of Lipo-SV as potent intranasal vaccine adjuvants to enhance antigen-specific mucosal immune response. Lipo-SV increase their uptake by the nasal ECs and inhibit the geranylgeranylation of RAB5 and RAB7B GTPases by inhibiting the mevalonate pathway. ① Lipo-SV reduce the degradation of antigens in lysosomes through arrested maturation of endosomes, thus increasing the distribution of antigens in recycling endosomes (RE), endoplasmic reticulum (ER), and Golgi apparatus for enhanced transcytosis of antigens. ② Lipo-SV stimulate the nasal ECs to secrete chemokine CCL20 *via* the TLR4 pathway, which recruits more submucosal DCs for antigen uptake. ③ After capturing antigens, DCs mature and migrate to the CLNs, increasing antigen presentation and mucosal immune response of the i.n. subunit vaccine. EE, early endosomes; LE, late endosomes; pIgR, polymeric immunoglobulin receptor; TRMs, tissue-resident memory cells; SIgA, secretory IgA.

2. Materials and methods

2.1. *Ethics*

All animal experiments were conducted following protocols approved by the Institutional Animal Care and Use Committee (IACUC) of the School of Pharmaceutical Sciences, Fudan University (Approval Nos.: 2019-08-YJ-LW-01 and 2024-03-YJ-LW-41). For the animal experiments, mice that lost more than 20% of their body weight were euthanized according to the IACUC guidelines. The experiment of virus challenge and all the viruses and infectious samples were conducted under enhanced biosafety level 2 (BSL-2) laboratory conditions.

2.2. Preparation and characterization of the drug-loaded liposomes

Lipo-SV were prepared by the thin-film hydration technique. Briefly, 1,2-dipalmitoyl-*sn*-glycerol-3-phosphocholine (DPPC), cholesterol (Chol), 1,2-distearoyl-*sn*-glycero-3-phosphoethanolamine-*N*-[methoxy (polyethylene glycol)-2000] (DSPE-mPEG$_{2000}$), and SV were dissolved in chloroform at a ratio of 125:93:4.2:12, then placed in a rotary evaporator to remove the organic solvent. The lipid film was hydrated with phosphate buffer solution (PBS) and extruded through a 200 nm polycarbonate membrane (Whatman, Cat#10417006, Maidstone, UK).

The liposomes loading RBD, HA1, or chicken ovalbumin (OVA) were prepared by a reverse-phase evaporation method. The lipid materials were dissolved in 3 mL of chloroform at a molar ratio of 125:93:4.2 (DPPC: chol: DSPE-mPEG$_{2000}$) and mixed with 1 mL of antigen solution (0.5 mg). The mixture was sonicated in a water bath to form a stable water-in-oil emulsion, followed by the removal of the organic solvent on a rotary evaporator. The emulsion was hydrated with PBS and then extruded through a 200 nm polycarbonate membrane. For the preparation of SV and RBD co-loaded liposomes (Lipo-SV-RBD), the above lipids and SV were dissolved in 3 mL of chloroform at a molar ratio of 125:93:4.2:12 (DPPC: chol: DSPE-mPEG$_{2000}$: SV) and mixed with 1 mL of RBD solution (0.5 mg). The liposomes were also prepared using the reverse-phase evaporation method. Particle size, polymer dispersity index (PDI), and zeta-potential of the liposomes were measured by dynamic light scattering (DLS, Zetasizer Nano ZS90, Malvern Instruments, Malvern, UK). The morphology of liposomes was examined by cryo-transmission electron micrograph (Cryo-TEM, FEI Tecnai G2 F20, 200 kV, FEI, Hillsboro, OR, USA).

2.3. Mouse immunization

For RBD antigens, BALB/c mice were i.n. inoculated with 50 μL PBS, RBD, Lipo-RBD, Lipo-SV-RBD, Lipo-SV plus Lipo-RBD, or CTB-RBD on Days 1, 22, and 210, respectively. For i.m. immunization, the mice were injected bilaterally in the quadriceps femoris with a total volume of 100 μL of PBS, RBD, Lipo-RBD, Lipo-SV-RBD, Lipo-SV plus Lipo-RBD, or Al(OH)$_3$-RBD on Days 1, 22, and 210, respectively. In Lipo-SV-treated groups, the mice were pretreated with Lipo-SV for 24 h before the immunization of Lipo-RBD. For intratracheal (i.t.) immunization, mice received 50 μL of PBS, RBD, Lipo-RBD, or Lipo-SV-RBD on Days 1 and 22, respectively. For the combination group of the i.t. immunization, Lipo-SV was i.n. administered 24 h prior to the i.t. immunization with Lipo-RBD. The RBD dose antigen for i.n. or i.m. immunization was 10 μg. The dose of Al(OH)$_3$ was 20 μg. The dose of RBD antigen for i.t. immunization was 1 μg.

For HA1 antigens, BALB/c mice were i.n. inoculated with 50 μL PBS, Lipo-SV (20 μg) plus Lipo-HA1 (10 μg) or CTB-HA1(containing 10 μg HA1 and 10 μg CTB) every 3 weeks for three times. In Lipo-SV-treated groups, the mice were pretreated with Lipo-SV for 24 h before the immunization with Lipo-HA1. For i.m. immunization, the mice were injected bilaterally in the quadriceps femoris with a total volume of 100 μL containing 10 μg HA1 and Al(OH)$_3$(2 mg/mL). The mice were euthanized to collect samples on Day 57 after the primary immunization. Blood was collected to separate sera at the indicated times from immunized mice. Nasal washes and bronchoalveolar lavage fluid (BALF) were obtained by washing the organs with 0.5 mL and 1.0 mL sterile PBS, respectively. Cerebrospinal fluid (CSF) was collected for analysis of inflammatory factor levels in the central nervous system (CNS). Lungs were minced into 2 mm × 2 mm pieces, digested with 1 mL of collagenase IV (2 mg/mL)/DNase I (5 mg/mL) at 37 °C for 60 min, and filtered through a 40-μm cell strainer (Falcon, Cat#352340, BD, Franklin Lakes, NJ, USA). CLNs and spleens were dissected from mice and processed into single-cell suspensions by passing the tissues through 40-μm cell strainers directly for analysis by flow cytometry (FCM).

2.4. Virus challenge

At 14 days after the third immunization, the vaccinated mice were anesthetized and then i.n. challenged with 10 times the murine median lethal dose (LD$_{50}$) of PR8 H1N1. Body weight and survival rates of infected mice were monitored daily after the challenge ($n = 5$). Mice that lost more than 20% of their initial body weight were humanely euthanized. The lungs and small intestines were collected for histopathological examination at 4 days post-infection ($n = 3$). For measuring viral loads, nasal washes and lungs were harvested at 4 days post-infection and stored at −80 °C until processed ($n = 4$). For detecting changes in immune cells after viral infection, the lungs and mediastinal lymph nodes (MLNs) were dissected and processed into single-cell suspensions for analysis by FCM at 4 days post-infection ($n = 3$).

2.5. Measurement of viral load in the mouse

Neuraminidase (NA) level, the main target of influenza antivirals, was detected by enzyme-linked immunosorbent assay (ELISA) in nasal washes and lung homogenates. Influenza viral titers in lungs were quantified using quantitative reverse transcription polymerase chain reaction (qRT-PCR) from the RNA samples. Briefly, frozen lungs collected as described above were homogenized in TRIzol (Thermo Fisher Scientific, Cat#15596026CN, Waltham, MA, USA) to isolate total RNA. Total RNA was reverse transcribed using Hifair III 1st Strand cDNA Synthesis Kit (gDNA digester plus) (Yeasen Biotech Co., Ltd., Cat#11139ES60, Shanghai, China). qRT-PCR analysis was conducted on a Bio-Rad CFX96 connect using an SYBR Green PCR kit (ABconal, Cat#RK21203, Woburn, MA, USA). β-actin served as an internal reference. The H1N1 influenza virus M gene and β-actin primers were used: (M gene: forward primer, 5′-AAGACCAATCCTGTC ACCTCTGA-3′; reverse primer, 5′-CAAAGCGTCTACGCTGCA GTC-3′; β-actin: forward primer, 5′-CCAGGTCATCACTATT GGCAAC-3′; reverse primer, 5′-TTTACGGATGTCAACGTCA-CAC-3′). Fold change of M gene mRNA was calculated using the $2^{-\Delta\Delta Ct}$ method comparing vaccine-treated mice to PBS-treated mice.

2.6. Detection of antigen-specific antibody titers

ELISA plates were coated with 100 μL of 1 μg/mL of RBD or HA1 protein overnight at 4 °C which were then blocked for 0.5 h at 37 °C using 5% bovine serum albumin (BSA) in PBS. The serial dilutions of serum or lavage fluid samples were added to the wells and incubated for 1 h at 37 °C. After being washed five times with PBS containing 0.05% Tween 20 (PBST), the plates were incubated with horseradish peroxidase (HRP)-conjugated IgG1, IgG, or IgA at 37 °C for 1 h. The plates were washed five times with PBST and incubated with 100 μL of 3,3',5,5'-tetramethylbenzidine (TMB) substrate. After stopping the reaction

with 50 μL of 2 mol/L H_2SO_4 solution in each well, optical density $(OD)_{450-570}$ was measured using a microplate reader (BioTek Instruments, Inc., Synergy 2, Winooski, VT, USA).

2.7. Hemagglutination inhibition (HAI) assays

To determine the serum or lavage fluid HAI titers, the samples were treated with receptor-destroying enzyme II (RDE II; Denka Seiken, Cat#340122, Tokyo, Japan) at 37 °C for 16 h. The enzyme activity was then inactivated by incubation for 30 min at 56 °C. The RDE-treated samples were serially diluted and incubated with four hemagglutination units (HAU) of PR8 H1N1virus in V-bottom 96-well plates at room temperature for 1 h. Thereafter, V-bottom 96-well plates were incubated with 0.5% chicken red blood cells at room temperature for 30 min.

2.8. Transepithelial cells study in vitro and in vivo

For the *in vitro* assay, different formulations were added into the upper compartment of the Calu-3 cell monolayer with the same concentration of liposomes loading Cy5-labeled OVA (Lipo-OVA-Cy5). Then, take all the basolateral compartment solution at the indicated time points and supplement with an equivalent volume of PBS. The maximum emission wavelength of the collected basolateral compartment solution was monitored using a microplate reader (BioTek Instruments, Inc.) at an excitation wavelength of 633 nm. For the GGPP-treated groups, the cells were incubated with GGPP (20 μmol/L) or GGPP plus Lipo-SV (10 μmol/L) for 24 h before the treatment with Lipo-OVA-Cy5 (20 μg/mL).

To estimate the effect of Lipo-SV on the transmucosal penetration of antigen *in vivo*, mice were i.n. administered with PBS or Lipo-SV. After 24 h, the mice were i.n. immunized with Lipo-OVA-Cy5 containing 10 μg of OVA. The mice were euthanized 30 min later. After removing the irrelevant affiliated tissues, the noses were fixed in 4% paraformaldehyde (PFA) for 24 h at 4 °C Next, the noses were decalcified for 7 days in decalcifying fluid (10% ethylenediaminetetraacetic acid (EDTA), pH 7.4) and then embedded in optimal cutting temperature compound (OCT, Sakura, Finetek, Tokyo, Japan) and frozen. Tissues were sliced into 8-μm sections for analysis of immunofluorescence.

2.9. Sodium dodecyl sulfate-polyacrylamide gel electrophoresis (SDS-PAGE) and western blotting assay

Protein quality was evaluated with 8%−12% SDS-PAGE under reducing conditions. The proteins in the gel were stained with Coomassie brilliant blue dye or transferred to nitrocellulose membranes (Cytiva, Cat#10401436, Marlborough, MA, USA). The membranes were blocked with 5% BSA-PBST and incubated with appropriate primary antibodies and HRP-conjugated secondary antibodies. The antibodies used were listed in Supporting Information Table S1. The specific protein bands in membranes were visualized using enhanced chemiluminescence buffer, and the images were captured by the Chemi Doc XRS system (Bio-Rad Laboratories, Hercules, CA, USA).

2.10. Subcellular distribution of Lipo-OVA

Calu-3 cells (1×10^5) were seeded in 35-mm glass-bottom dishes and pre-treated with or without Lipo-SV (10 μmol/L), RAB5 small interfering RNA (siRNA), or RAB7B siRNA for 24 h, followed by incubation with Lipo-OVA-Cy5 (10 μg/mL) for another 3 h. For the GGPP-treated groups, the cells were incubated with GGPP (20 μmol/L) plus Lipo-SV (10 μmol/L) for 24 h before the treatment with Lipo-OVA. The cells were washed with PBS and stained with different fluorescent organellar probes, including Lyso-tracker red (Beyotime, Cat#C1046, Shanghai, China), ER-tracker red (Beyotime, Cat#C1041S), or Golgi-tracker red (Beyotime, Cat#C1043) according to the manufacturer's instructions. The cell nuclei were stained with Hoechst 33342. In the RAB11A tracking group, cells were washed with PBS and fixed with 4% PFA at room temperature for 10 min. Then the cells were permeabilized with 0.3% Triton X-100 at room temperature for 10 min and blocked with 5% BSA (in PBS) at room temperature for 1 h. After incubating overnight at 4 °C with mouse anti-human RAB11A monoclonal antibody, the cells were incubated with Alexa Fluor 594-conjugated goat anti-mouse IgG secondary antibody at room temperature for 1 h and then incubated with 4′,6-diamidino-2-phenylindole (DAPI) at room temperature for 5 min. The cells were observed by a Leica TCS SP8 confocal microscope (Leica Microsystems, Wetzlar, Germany).

2.11. Nasal ciliotoxicity

To evaluate nasal ciliotoxicity, female Sprague−Dawley rats were i.n. inoculated with 100 μL PBS, Lipo-SV plus Lipo-HA1, CTB-HA1 and 1% sodium deoxycholate-HA1 for 24 h, respectively. Then, the nasal septal mucosa was removed, fixed with 2.5% glutaraldehyde, dehydrated with ethanol gradient, dried at CO_2 critical point, and sprayed with ion sputtering. Finally, the changes in cilia morphology were observed by scanning electron microscope (SEM, Hitachi High-Tech Corporation, Regulus 8100, Tokyo, Japan). In Lipo-SV-treated groups, the rats were pretreated with Lipo-SV for 24 h, followed by Lipo-HA1. The doses of SV, CTB, and HA1 were 100, 50, and 50 μg, respectively.

2.12. Statistical analysis

Data were presented as mean ± standard deviation (SD). Statistical significance was determined using GraphPad Prism 8.0 software (San Diego, CA, USA). An unpaired two-tailed *t*-test was used to analyze differences between two groups. One-way or two-way analysis of variance (ANOVA) with Tukey's multiple comparisons *post hoc* test was used to analyze differences among multiple groups. The results were considered significant when $P < 0.05$ ($^*P < 0.05$, $^{**}P < 0.01$, $^{***}P < 0.001$).

3. Results

3.1. Lipo-SV potentiated intranasal subunit vaccines to elicit robust systemic and local mucosal immune responses

Because of the poor solubility of lipophilic SV, i.n. administration of free SV may reduce their absorption by the nasal ECs, weakening the mucosal adjuvanticity. To address this issue, we prepared liposomes encapsulating SV, Lipo-SV, with a particle size of 140.13 ± 8.34 nm in diameter (Fig. 2A). The average size of Lipo-SV remained unchanged for 72 h, indicating that the formulation was stable (Supporting Information Fig. S1A). In addition to solubilization, the liposomal formulation exhibited a sustained release profile, evidenced by that around 16% of SV was released from Lipo-SV within 12 h in simulated nasal electrolyte solution

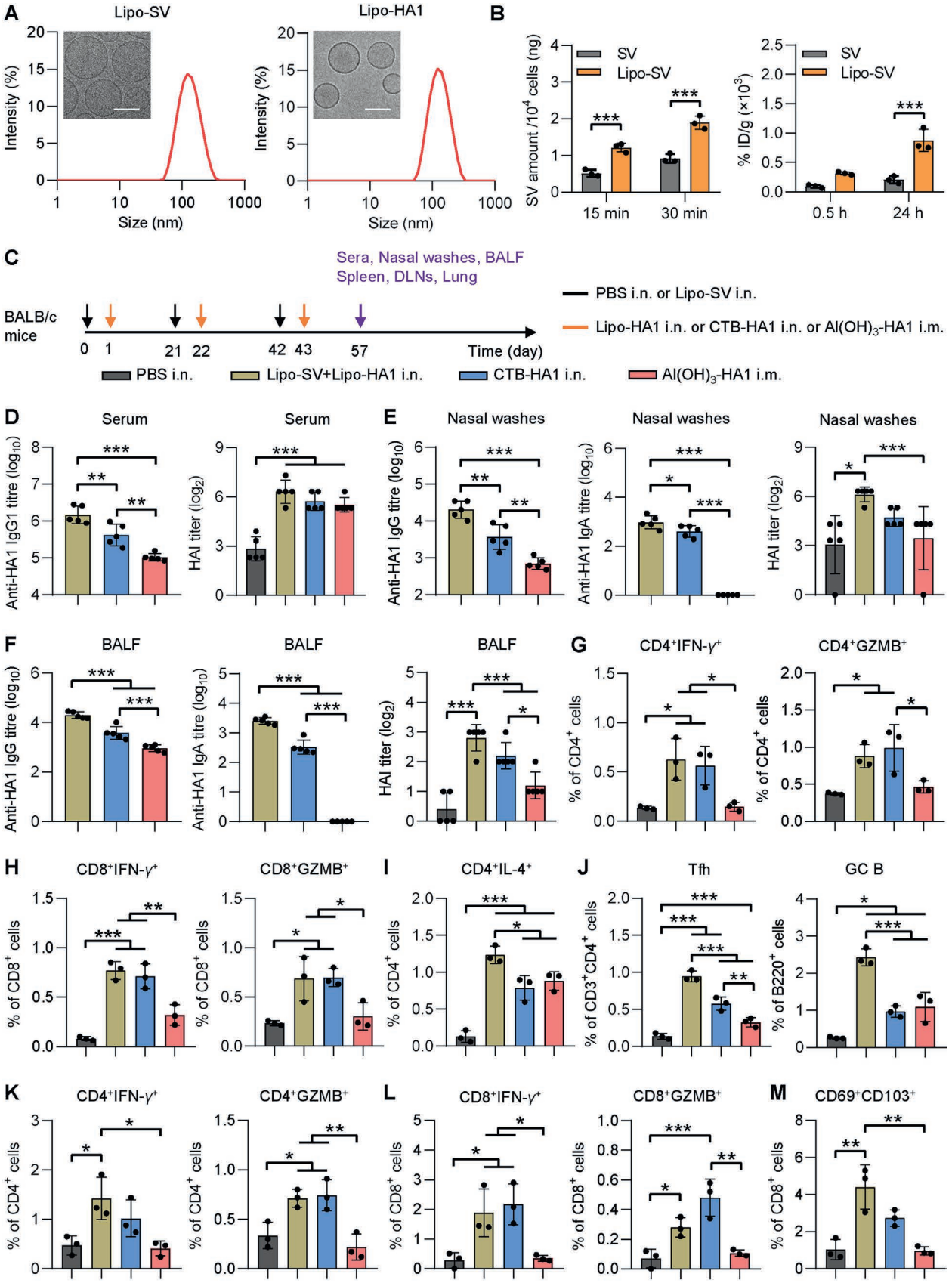

Figure 2 I.n. immunization of Lipo-SV combined with Lipo-HA1 enhanced HA1-specific systemic and mucosal immunity. (A) The size distribution and Cryo-TEM of Lipo-SV and Lipo-HA1, respectively. Scale bar = 100 nm. (B) The amount of SV in the Calu-3 cell monolayer (left) or nasal mucosa (right) at different times following administration of free SV or Lipo-SV (n = 3). % ID/g, percentage of the injected dose

(SNES), while around 36% was released in PBS 7.4 containing 0.5% sodium dodecyl sulfate (Fig. S1B). The accelerated release in the sodium dodecyl sulfate (SDS)-containing medium is attributed to the increased solubilization of SV by sodium dodecyl sulfate. The slow-release profile of drugs from the liposomes enhances drug stability and prolongs mucosal residence time[25]. This prolonged mucosal exposure of SV is critical for achieving a robust and durable therapeutic response. Compared with free SV, liposomes significantly increased the uptake of SV in the Calu-3 cell monolayer and nasal mucosa, respectively (Fig. 2B), indicating that liposomes can enhance transmucosal penetration of SV. Specifically, after 24 h following i.n. administration of Lipo-SV, the distribution of SV in the nasal mucosa was 4.3-fold as high as that of free SV. Among all the tissues or organs investigated, the concentration of SV was the highest in the nasal mucosa (Supporting Information Fig. S2). The particle sizes of Lipo-RBD and liposomes loading SV and RBD (Lipo-SV-RBD) were 117.3 $\pm$ 2.95 and 135.03 $\pm$ 3.27 nm in diameter, respectively (Supporting Information Fig. S3A and Table S2). Both RBD liposomal vaccines were stable in PBS and serum (Fig. S3B).

The dose of RBD antigen of i.t. immunization of Lipo-RBD was 1 μg, whose dose was equivalent to the dose deposited in the lung through i.n. administration of 10 μg of Lipo-RBD (Supporting Information Figs. S4 and S5). The result showed that Lipo-SV-RBD induced significantly lower IgG1 antibody titers compared to immunization with Lipo-SV and Lipo-RBD separately (Supporting Information Fig. S6). Previous study reported that it took 24 h for SV to inhibit the geranylgeranylation of small GTPases, including RAB5 in APCs, resulting in arrested endosomal maturation[23]. Therefore, i.n. administration of Lipo-SV 24 h prior to Lipo-RBD ensured enough time for inhibiting the geranylgeranylation of RAB5 and RAB7B GTPases in nasal ECs. I.n. immunization with Lipo-SV combined with Lipo-RBD elicited a higher level of the RBD-specific systemic IgG1 antibody than the i.m. injection of RBD vaccines with aluminum adjuvant ($Al(OH)_3$-RBD) or the i.t. immunization of Lipo-SV combined with Lipo-RBD at Day 35 by 1.8-fold and 5-fold, respectively. At Day 217, the i.n. immunization with Lipo-SV combined with Lipo-RBD induced IgG1 antibody by 5.7-fold of that before the booster immunization (Fig. S6). This data demonstrated that mice i.n. immunized with Lipo-SV combined with Lipo-RBD exhibited a long-lasting systemic IgG1 antibody response. The i.n. immunization group induced IgA and IgG antibody responses in nasal washes and BALF compared with i.m. immunization (Supporting Information Fig. S7). Furthermore, Lipo-SV combined with Lipo-RBD increased $CD8^+$ TRMs ($CD8^+CD69^+CD103^+$) in the lungs after i.n. immunization at Day 217 by 3.6-fold, 2.2-fold and 3.7-fold compared with the PBS control, CTB-RBD and $Al(OH)_3$-RBD (Supporting Information Fig. S8). These results demonstrated that Lipo-SV plus Lipo-RBD elicited long-term tissue resident memory T cells. Taken together, these results showed that i.n. immunization of Lipo-SV combined with Lipo-RBD induced both long-acting serum antibody response and local mucosal antibody response, while i.m. injection of Lipo-SV combined with Lipo-RBD or $Al(OH)_3$-RBD had insufficient ability to induce mucosal antibody response.

To assess the adjuvanticity of Lipo-SV to the Lipo-HA1 vaccine, we purified HA1 proteins of PR8 H1N1 influenza from *Escherichia coli* and i.n. immunized mice with Lipo-SV combined with Lipo-HA1 three times (Supporting Information Fig. S9). The mice received i.n. administration of the HA1 vaccine with the mucosal adjuvant CTB (CTB-HA1) or i.m. immunization of the HA1 vaccine with the aluminum adjuvant ($Al(OH)_3$-HA1) were used for comparison (Fig. 2C). I.n. immunization with Lipo-SV plus Lipo-HA1 increased the serum IgG1 antibody titers, IgA antibody titers in nasal lavage fluid, and IgA antibody titers in BALF by 15.7-fold, 1115-fold, and 2592-fold in comparison with i.m. injection of $Al(OH)_3$-HA1, respectively (Fig. 2D−F). I.n. immunization with Lipo-SV combined with Lipo-HA1 induced higher levels of HAI titers in lavage fluids than i.m. injection of $Al(OH)_3$-HA1 (Fig. 2E and F). Taken together, these results demonstrated that i.n. immunization with Lipo-SV combined with Lipo-HA1 generated robust systemic IgG1 and mucosal IgA antibody responses. Although i.m. immunization with $Al(OH)_3$-HA1 produced a strong systemic antibody response, it failed to induce mucosal antibody responses.

I.n. immunization with Lipo-SV combined with Lipo-HA1 significantly induced the amount of activated ($CD69^+$) $CD4^+$ T cells and $CD8^+$ T cells, which were 1.8-fold and 2.0-fold of those of the i.m. immunization group with $Al(OH)_3$-HA1, respectively (Supporting Information Fig. S10). Moreover, Lipo-SV facilitated Lipo-HA1 to induce stronger Th1, Th2, and CTLs responses than $Al(OH)_3$ adjuvant, evidenced by the significantly higher frequencies of $CD4^+$interferon-gamma (IFN-γ)$^+$, $CD8^+$IFN-γ^+, $CD4^+$granzyme B (GZMB)$^+$, $CD8^+$GZMB$^+$, and $CD4^+$IL-4$^+$ in the i.n. Lipo-SV group (Fig. 2G−I and Supporting Information Fig. S11). The Lipo-SV combined with Lipo-HA1 increased central memory ($CD8^+CD44^+CD62L^+$) and effector memory ($CD8^+CD44^+CD62L^-$) T cells in the spleen after i.n. immunization by 1.27-fold and 1.50-fold compared with the PBS control, respectively (Supporting Information Fig. S12). Taken together, these results demonstrated that Lipo-SV potentiated the liposomal subunit vaccines to elicit strong Th1, Th2 immunity, and CTLs responses, while $Al(OH)_3$ adjuvanted the vaccines to enhance Th2 immunity but with insufficient Th1 immunity or CTLs responses.

Germinal center (GC) formation is critical for the generation of strong and long-term humoral immunity, and the affinity selection of GC B cells is dependent on T follicular helper cells (Tfh)[26]. The frequencies of Tfh ($CD4^+CXCR5^+PD\text{-}1^+$) and GC B ($B220^+GL7^+Fas^+$) cells in the draining lymph nodes (DLNs) were all markedly increased in mice i.n. administered with Lipo-SV combined with Lipo-HA1, which was increased by 1.9-fold and 1.2-fold compared with those i.m. immunized with $Al(OH)_3$-HA1, respectively (Fig. 2J and Supporting Information Fig. S13). These data demonstrate that Lipo-SV facilitated Lipo-HA1 vaccines to produce higher levels of humoral immune responses.

per g tissue. (C) Scheme of immunization and sampling regimens. The dose of HA1 was 10 μg. (D) Anti-HA1 IgG1 titers and HAI titers in serum, respectively ($n = 5$). (E, F) Anti-HA1 IgG titers, Anti-HA1 IgA titers, and HAI titers in nasal washes (E) and BALF (F), respectively ($n = 5$). (G−I) IFN-γ and granzyme B produced by $CD4^+$ T and $CD8^+$ T cells (G, H) and IL-4 produced by $CD4^+$ T cells (I) by FCM, respectively ($n = 3$). (J) The percentages of Tfh and GC B cells in the DLNs by FCM, respectively ($n = 3$). (K, L) The expression of IFN-γ and granzyme B in $CD4^+$ T and $CD8^+$ T cells in the lung by FCM, respectively ($n = 3$). (M) The percentages of $CD8^+$ TRMs in the lung by FCM ($n = 3$). Data are presented as mean $\pm$ SD. Statistical significance was assessed by one-way or two-way ANOVA with Tukey's *post hoc* test for multiple groups. $^*P < 0.05$, $^{**}P < 0.01$, $^{***}P < 0.001$ *vs.* indicated.

A notably high percentage of IFN-γ or GZMB generating $CD4^+$ T and $CD8^+$ T cells was observed in the lungs of mice i.n. immunized with Lipo-SV combined with Lipo-HA1 or CTB-HA1 (Fig. 2K and L, Supporting Information Fig. S14A and S14B). In contrast, mice i.m. immunized with $Al(OH)_3$-HA1 failed to produce IFN-γ and granzyme B in $CD4^+$ T and $CD8^+$ T cells, respectively. $CD8^+$ TRMs in the lungs are essential to defend against viral infection[27]. Mice i.n. immunized with Lipo-SV combined with Lipo-HA1 significantly increased the frequencies of $CD8^+CD69^+CD103^+$ ($CD8^+$ TRMs) cells in the lungs by 4.6-fold in comparison with the groups i.m. immunized with $Al(OH)_3$-HA1(Fig. 2M and Fig. S14C). These data suggested that i.n. immunization with Lipo-SV combined with Lipo-HA1 or CTB-HA1, but not i.m. immunization with $Al(OH)_3$-HA1, induced T-cell immunity in the lung.

3.2. Lipo-SV enhanced the immune protection of the intranasal Lipo-HA1 vaccine against PR8 H1N1 influenza virus infection

To evaluate the efficacy of various vaccines plus adjuvants against the viral infection, the vaccinated mice were challenged with a $10 \times LD_{50}$ dose of the PR8 H1N1 virus at 14 days after the third immunization. In the control group, the mice treated with PBS lost their body weight more than 15% at 5 days post the virus challenge, causing the death of all five mice at Day 6 (Fig. 3A and Supporting Information Fig. S15). Comparatively, all the HA1 vaccine-treated mice survived during the 12 days of observation post viral challenge with less than 10% reduction in the average body weights. Specifically, the mice treated with i.n. Lipo-SV combined with Lipo-HA1 exhibited the least weight loss among all three vaccine groups (Fig. 3A and Fig. S15). Besides, H1N1 infection can cause pulmonary edema and inflammation in mice with an increase in lung tissue weight. So, the lung index is an indicator to measure the extent of lung impairment[28]. At 4 days post-infection, the lung index of the group of i.n. Lipo-SV plus Lipo-HA1 was significantly smaller than that of the PBS group (Supporting Information Fig. S16), suggesting that Lipo-SV combined with Lipo-HA1 treatment could diminish the virus-induced pulmonary edema. The NA levels of nasal washes or lungs in mice treated with i.n. Lipo-SV combined with Lipo-HA1 was similar to that with i.n. CTB-HA1, but significantly lower than that with PBS or $Al(OH)_3$-HA1 (Fig. 3B). qRT-PCR results showed that the viral matrix (M) gene RNA level in the lung tissue of the i.n. Lipo-SV plus Lipo-HA1 group was only 1/6 of that of the i.m. $Al(OH)_3$-HA1 group (Fig. 3C). These results demonstrated that the i.n. immunization with Lipo-SV combined with Lipo-HA1, but not the i.m. immunization with $Al(OH)_3$-HA1, remarkably attenuated the replication of the H1N1 virus both in the nose and lung of mice.

Hematoxylin-eosin (H&E) staining of the lung sections of PBS control mice challenged with PR8 H1N1 showed severe pathological changes, including alveolitis with mixed inflammatory cell infiltrates, pulmonary edema and pulmonary congestion (Fig. 3D). The mice receiving $Al(OH)_3$-HA1 at 4 days post infection did not significantly reduce the lung inflammation compared with the control (Fig. 3D). In contrast, the mice i.n. immunized with Lipo-SV plus Lipo-HA1 or with CTB-HA1 showed markedly attenuated inflammatory response in the lung, such as reduced neutrophil infiltration and pneumonia. Furthermore, the interleukin (IL)-6, tumor necrosis factor-alpha (TNF-α), IL-1β, and CCL2 levels were 0.28-, 0.56-, 0.33-, and 0.13-fold in the lung of mice i.n. immunized with Lipo-SV plus Lipo-HA1 compared with PBS, respectively (Fig. 3E). Collectively, these results illustrated that the i.n. immunization with Lipo-SV combined with Lipo-HA1 rather than the i.m. immunization with $Al(OH)_3$-HA1 decreased lung inflammation caused by the H1N1 infection.

Next, the immune cells in the MLNs and lungs of mice from different groups were analyzed after challenge with PR8 H1N1. At 4 days post challenge, the mice with i.n. immunization of Lipo-SV plus Lipo-HA1 showed the populations of $CD11c^+$ DCs, $CD19^+$ B cells, and $CD4^+$ T cells in the MLNs increased by 5.20-, 1.82-, and 1.17-fold in comparison to those of the PBS control, respectively (Supporting Information Figs. S17 and S18). The mice i.n. immunized with Lipo-SV combined with Lipo-HA1 exhibited the most significant number of CD4 T^+ and CD8 T^+ cells expressing IFN-γ and granzyme B in the MLNs compared with other groups, demonstrating the activation of antigen-specific T-cell immunity in the MLNs (Fig. 3F, Supporting Information Figs. S19 and S20). Moreover, the number of $CD4^+$ T and $CD8^+$ T cells in the lung of mice i.n. immunized with Lipo-SV combined with Lipo-HA1 were the highest among all the groups, respectively (Supporting Information Fig. S21). The proportions of $CD4^+$IFN-γ^+, $CD4^+GZMB^+$, $CD8^+$IFN-γ^+, and $CD8^+GZMB^+$ T cells, which were essential for preventing viral infections, were significantly raised in mice immunized with Lipo-SV combined with Lipo-HA1 compared with those of other groups (Fig. 3G, Supporting Information Figs. S22 and S23). By contrast, we failed to detect an increase in these cells in the lungs of $Al(OH)_3$-HA1 vaccinated mice after being challenged by the PR8 H1N1 (Fig. 3G, Figs. S22 and S23). These data suggest that the protective effect observed in vaccinated mice was related to the cellular immune responses.

Studies have shown that H1N1 infection can cause intestinal injury[29,30]. Therefore, the protective effect of the vaccine on the intestine was evaluated. As shown in Supporting Information Fig. S24A, compared with other groups, i.n. immunization of Lipo-SV combined with Lipo-HA1 significantly alleviated the reduction in colon length. The H&E-stained sections further revealed that i.n. immunization with Lipo-SV combined with Lipo-HA1 resulted in less rupture of intestinal villi and less infiltration of inflammatory cells (Fig. S24B). Compared with CTB-HA1 and $Al(OH)_3$-HA1, Lipo-SV combined with Lipo-HA1 ameliorated intestinal injury caused by H1N1 infection in mice.

3.3. Lipo-SV enhanced transmucosal penetration of antigen

To evaluate the penetration of antigens across the nasal mucosa, the vaccine of liposomes loading the model antigen OVA (Lipo-OVA) was prepared (Supporting Information Fig. S25A). About 17% and 21% of OVA was released from the liposomes within 12 h in PBS and SNES, respectively (Fig. S25B). Circular dichroism (CD) spectroscopy was employed to assess the stability of the OVA encapsulated in liposomes. The results demonstrated that the secondary structure of OVA released from the liposomes was similar to that of the free OVA, evidenced by the conserved double negative peaks of the α-helix at 208 and 222 nm without observable spectral shifts (Fig. 4A). Confocal laser scanning microscopy (CLSM) images showed that i.n. Lipo-SV significantly enhanced the nasal mucosal permeability of antigens (Fig. 4B). The Lipo-SV-enhanced transcytosis of Lipo-OVA across the nasal ECs was specifically inhibited by chlorpromazine, suggesting the clathrin-mediated transcytosis of Lipo-OVA (Supporting Information Fig. S26). In addition, the Calu-3 cell monolayer, as a

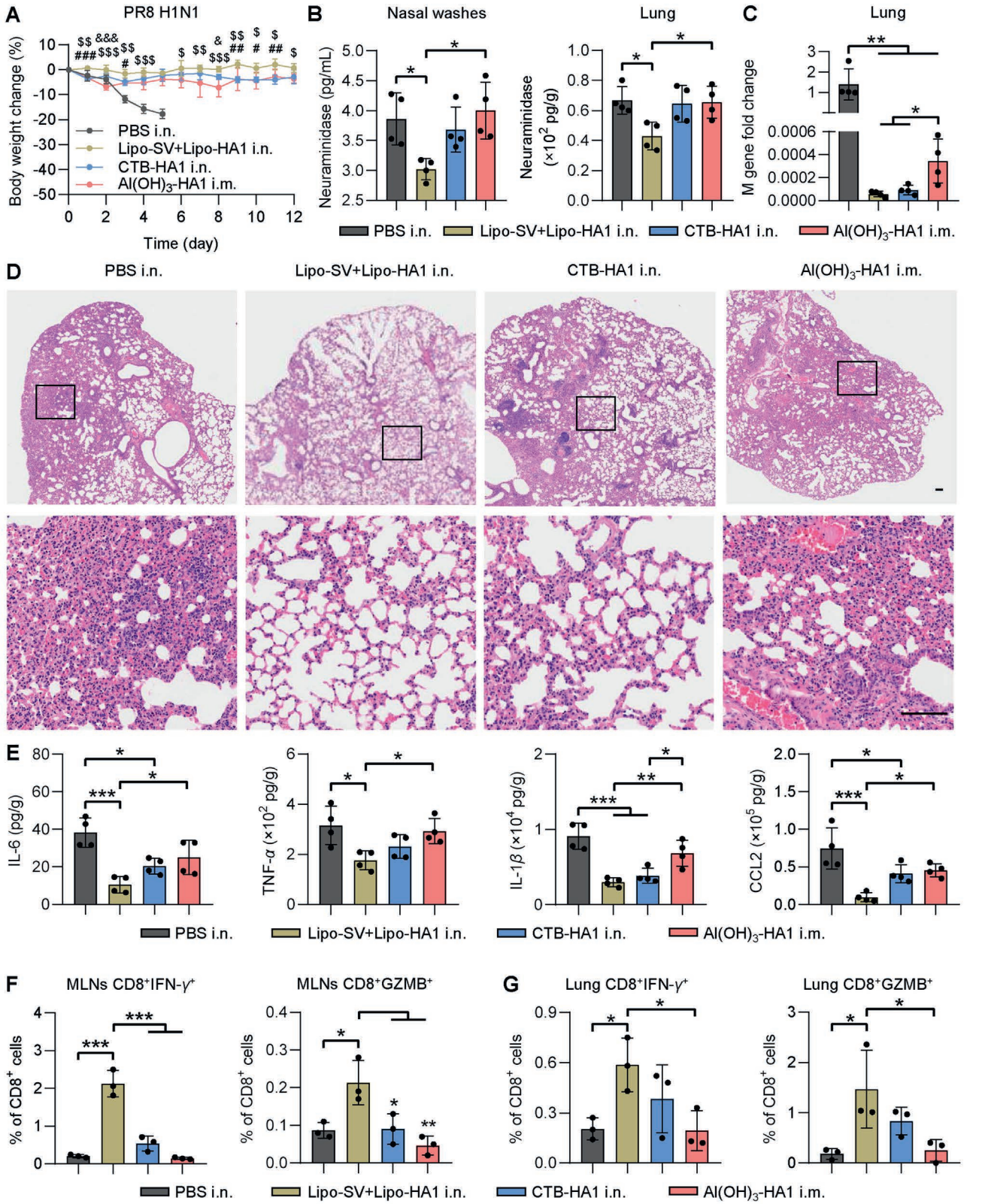

Figure 3 I.n. immunization of Lipo-SV combined with Lipo-HA1 protected mice against H1N1 influenza virus infection. (A) Body weight changes ($n = 5$) of mice after PR8 H1N1 influenza virus challenge. BALB/c mice were i.n. or i.m. immunized with different vaccines every 3 weeks for three times. The mice were inoculated i.n. challenged with PR8 H1N1 ($10 \times LD_{50}$) on Day 57 after the first dose of immunization. The day of the virus infection in mice was designated Day 0. (B) Neuraminidase (NA) activity in nasal washes and lungs ($n = 4$) was determined by ELISA. (C) Relative expression levels of H1N1 influenza virus matrix (M) gene viral RNA ($n = 4$) in the lung of immunized mice compared to

traditional method to study permeability across cell barriers, is used to evaluate the ability of Lipo-SV to enhance the transepithelial transport of antigen[31,32]. The cell monolayer with the transepithelial electrical resistance (TEER) of 500 Ω cm^2 was used in the experiment (Fig. 4C). The positive staining of tight junction-related protein ZO-1 and OCCLUDIN in continuous boundaries between Calu-3 cells further supported the formation of the monolayer (Supporting Information Fig. S27). After confirming the feasibility and availability of Lipo-SV and Lipo-OVA (Supporting Information Fig. S28). Lipo-SV increased the transcellular transport of Lipo-OVA at 180 min by 2.1-fold compared with Lipo-OVA alone (Fig. 4D). Lipo-SV increased the apparent permeability coefficient (P_{app}) of Lipo-OVA, which is defined as the rate of the liposomes crossing a Calu-3 monolayer on a Transwell membrane, by 2.44-fold in comparison with Lipo-OVA alone (Fig. 4E). However, such enhancement of the antigen transport across the monolayer of Lipo-SV was blocked by the co-administration of Lipo-SV with GGPP (Fig. 4D and E). These results suggested that Lipo-SV increased liposomal antigen transport across the nasal mucosa and Calu-3 monolayer by inhibiting the MVA pathway.

Trafficking and cargo sorting on the early and late endocytic pathway are closely related to the RAB5 GTPase-expressed early endosomes and the RAB7 GTPase-expressed late endosomes activity, respectively[23,33]. Lipo-SV decreased the amount of RAB5 localized on the membrane of Calu-3 cells, resulting in arrested endosomal maturation (Fig. 4F). The amount of membrane RAB7B was reduced due to a slower transition from endosome to late endosome (Fig. 4G). Co-administration of Lipo-SV with GGPP restored the cellular distribution of RAB5 and RAB7B to the untreated normal level, respectively (Fig. 4F and G). Further, intracellular trafficking analysis by CLSM (TCS-SP8, Leica, Wetzlar, Germany) demonstrated that most of Lipo-OVA colocalized with lysosomes following the internalization (Supporting Information Fig. S29). Lipo-SV pretreatment reduced the extent of such lysosomal colocalization, but increased colocalization of the liposomal antigen with the recycling endosome, endoplasmic reticulum, and Golgi apparatus (Supporting Information Figs. S29−S32). Whereas, the addition of GGPP plus Lipo-SV recovered the lysosomal distribution of Lipo-OVA (Fig. S29). To test whether RAB5 or RAB7B was involved in the regulation of antigen intracellular transport, we inhibited the expression of RAB5 or RAB7B in Calu-3 cells by transient transfection of RAB5 or RAB7B siRNA. The Western blot assay revealed that RAB5 protein levels in the RAB5 siRNA group decreased to 25% of those in cells transfected with the corresponding scrambled siRNA (Ctrl siRNA, Supporting Information Fig. S33). Knockdown of RAB5 *via* siRNA transfection resulted in a reduction in the colocalization of the liposomal antigen with lysosomes, which was consistent with the result of the Lipo-SV-treated group (Fig. 4H and I). The RAB7 siRNA transfection showed a reduced lysosomal colocalization with liposomal antigen similar to the Lipo-SV pretreatment (Supporting Information Figs. S34 and S35). The observed reduction in lysosomal targeting of antigens through impairment of the RAB5/RAB7B pathway provides supporting evidence of redirecting antigens away from degradative pathways. This result, combined with the data of blocked transcytosis by GGPP, supported that RAB5/RAB7B geranylgeranylation plays a crucial role in regulating antigen trafficking. Addition of an ER/Golgi pathway inhibitor (brefeldin A, BFA), or a Golgi/recycling endosome compartment (REC)/plasma membrane (PM) pathway inhibitor (monensin, MON) slowed down the transcytosis, indicating that antigen transmembrane transport was associated with the ER/Golgi pathway (Supporting Information Fig. S36). Taken together, Lipo-SV diminished the lysosomal distribution of Lipo-OVA with reduced antigen degradation and increased antigen transcytosis by inhibiting the geranylgeranylation of small GTPases such as RAB5 and RAB7B in the Calu-3 cells.

3.4. Lipo-SV increased DCs recruitment in the nasal mucosa through the TLR4-dependent pathway

Submucosal DCs are professional APCs that act as "sentinels" to patrol under the epithelial layer[34,35]. Recruitment of submucosal DCs is a critical step to trigger subsequent adaptive immune responses. After i.n. administration of Lipo-SV for 24 h, more DCs were recruited to the submucosal lamina propria compared to the PBS control (Fig. 5A). The Western blotting results showed that Lipo-SV decreased the amount of RAB7B localized in the Calu-3 membranes (Fig. 4G). Whereas the decrease in membrane distribution of RAB7B was restored by GGPP. RAB7B has been reported to be a negative regulator of TLR4 *via* promoting TLR4 to lysosomes for degradation[36]. To better understand the molecular cues for DCs recruitment, we assessed the expression of TLR4 on Calu-3 cells after treatment with Lipo-SV for 24 h. The result demonstrated that Lipo-SV increased the TLR4 level in Calu-3 cells (Fig. 5B). The expression of TLR4 could not be increased when the concentration of Lipo-SV was lower than 5 μmol/L and the incubation time of Lipo-SV was less than 12 h (Supporting Information Fig. S37). Both immunofluorescence images and FCM analysis showed that the expression of TLR4 was increased on nasal ECs after i.n. administration of Lipo-SV for 24 h (Fig. 5C and D, Supporting Information Fig. S38). Moreover, co-administration of Lipo-SV with TLR4 inhibitor M62812 reduced the expression of TLR4 to normal levels. The expression level of TLR4 reverted to PBS level after co-administration of Lipo-SV with GGPP (Fig. 5E). Collectively, Lipo-SV increased the amount of TLR4 on nasal ECs by inhibiting the formation of GGPP that was required for geranylgeranylation of RAB7B GTPases.

CCL20 is known to be secreted by mucosal ECs in response to TLR stimulation, which attracts the immature DCs to ECs[37]. We tested the secretion of CCL20 in the chamber solution of Calu-3 cell monolayer after treatment with PBS or Lipo-SV for 24 h. The results showed that Lipo-SV treatment increased the secretion

those of PBS-immunized mice were measured by qRT-PCR. (D) Representative histopathological changes in the H&E-stained lung tissues ($n = 3$). Scale bar = 100 μm. (E) The IL-6, TNF-α, IL-1β, and CCL2 levels in the lungs at 4 days post-infection were determined by ELISA ($n = 4$). (F, G) IFN-γ and granzyme B produced by T cells in the mediastinal lymph nodes (MLNs) (F) and lungs (G) were analyzed by FCM ($n = 3$). Data are presented as mean ± SD. Statistical significance was assessed by one-way or two-way ANOVA with Tukey's *post hoc* test for multiple groups. #, significant difference between Lipo-SV + Lipo-HA1 group and CTB-HA1 group. $, significant difference between Lipo-SV + Lipo-HA1 group and $Al(OH)_3$-HA1 group. &, significant difference between CTB-HA1 group and $Al(OH)_3$-HA1 group. $^*P < 0.05$, $^{**}P < 0.01$, $^{***}P < 0.001$ *vs*. indicated.

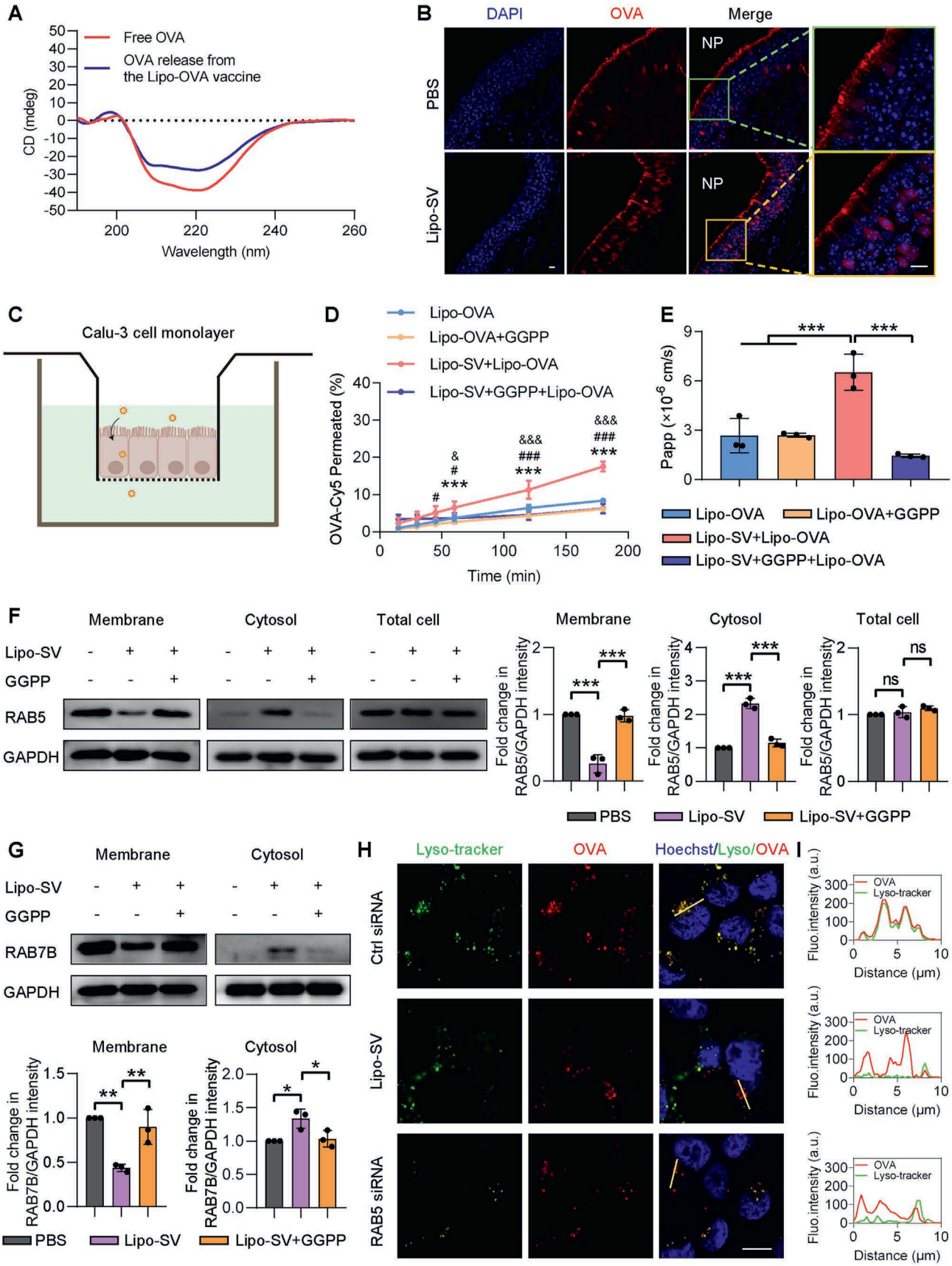

Figure 4 Lipo-SV increased the transcytosis of antigen by inhibiting the mevalonate pathway. (A) CD spectra of free OVA and OVA released from Lipo-OVA. (B) Fluorescence micrograph of the murine nasal cavity after i.n. immunization of Lipo-OVA-Cy5 for 0.5 h. In the Lipo-SV-

of CCL20 by 1.5-fold compared with the PBS group (Fig. 5F). The results by FCM showed that the number of recruited DCs induced by Lipo-SV was significantly increased by approximately 5.5-fold compared to that of the control (Fig. 5G and Supporting Information Fig. S39). Notably, M62812 inhibited the Lipo-SV-induced CCL20 secretion, resulting in the number of submucosal $CD11c^+$ DC recruitment decreased to the control level. These results demonstrated that Lipo-SV stimulated nasal ECs to secrete CCL20 through a TLR4-dependent pathway to recruit submucosal DCs.

3.5. Lipo-SV promoted DCs maturation and antigen presentation

Immunofluorescence micrographs showed that Lipo-SV increased the number of OVA-loaded submucosal DCs in BALB/c mice (Fig. 6A). Antigen-loaded DCs migrate to DLNs for triggering subsequent adaptive immune response in the mucosal immune system[17]. After i.n. immunization of Lipo-SV for 24 h and subsequent Lipo-OVA for another 18 h, the number of migratory DCs in the CLNs and the OVA-loaded DCs that migrated into the CLNs were increased by 1.7-fold and 2.1-fold compared with those of mice receiving i.n. Lipo-OVA alone, respectively (Fig. 6B). The immunofluorescence micrograph further depicted that Lipo-SV could increase the number of migratory DCs in the CLNs and the OVA-loaded DCs that migrated into the CLNs (Fig. 6C). Notably, more antigens were distributed in the T-zone and T-B border of the CLNs in the Lipo-SV plus Lipo-OVA group, which was 3.6-fold and 7.8-fold of those in the Lipo-OVA group, respectively (Supporting Information Fig. S40). The results of the experiment on antigen transport in C57BL/6 mice showed that Lipo-SV promoted *trans*-nasal epithelial transport of Lipo-OVA and submucosal DCs recruitment (Supporting Information Fig. S41A). Lipo-SV also increased the number of OVA-loaded DCs that migrated into the CLNs in C57BL/6 mice (Fig. S41B). These results, in line with the findings in BALB/c mice, demonstrated that the Lipo-SV's ability to increase transcytosis of antigens and submucosal DCs recruitment and delivery of antigens in the draining lymph nodes.

The ability of Lipo-SV to simulate the DCs activation was analyzed using primarily cultured bone marrow-derived dendritic cells (BMDCs) from C57BL/6 mice. The surface expression of costimulatory molecules CD40, CD80, CD86, and MHC II was remarkably upregulated in the group of Lipo-SV combined with Lipo-OVA compared to other groups (Supporting Information Fig. S42A). Lipo-SV increased the antigen presentation capability by detecting the percentage of $OVA_{257\text{-}264}$ (SIINFEKL) peptide bound to $H\text{-}2K^b$ on $CD11c^+$ cells, which was 12.6-fold, 7.3-fold, and 1.6-fold compared with the PBS group, Lipo-SV group, and Lipo-OVA group, respectively (Fig. S42B). In addition, Lipo-SV combined with Lipo-OVA induced BMDCs to secrete the highest amount of TNF-α, which was 9.5-fold, 7.3-fold, and 1.7-fold in comparison with the PBS group, Lipo-SV alone group, and Lipo-OVA alone group, respectively (Fig. S42C). It is noted that Lipo-SV alone did not alter the expression of the above phenotypic markers and the expression of the cytokines in the absence of antigen exposure. Taken together, the up-regulated number of costimulatory molecules on BMDCs surface, antigen presentation, and enhanced expression of the cytokines indicated that the combination of Lipo-SV and Lipo-OVA was crucial to stimulate the intense DCs maturation and antigen presentation. We next assessed the DCs maturation and antigen presentation in the total DCs, migratory DCs, and resident DCs in the CLNs following different treatments. FCM results displayed that i.n. Lipo-SV combined with Lipo-OVA increased the expression of costimulatory molecules on the surface of DCs and antigen presentation in the CLNs (Supporting Information Fig. S43A). In addition, only the expression of MHC II in the resident DCs in the CLNs was increased in the group of Lipo-SV combined with Lipo-OVA compared with the control. Whereas, the expression of CD40, CD80, and MHC II on $CD11C^+$ cells were upregulated in the group of Lipo-SV plus Lipo-OVA in the migratory DCs in the CLNs compared with the control. Lipo-SV plus Lipo-OVA increased the percentage of $H\text{-}2K^b$-SIINFEKL on $CD11c^+$ cells by 15.4-fold, 7.4-fold, and 2.4-fold in comparison with the PBS group, Lipo-SV alone group, and Lipo-OVA alone group, respectively (Fig. S43B and Fig. 6D). Taken together, these data demonstrated that Lipo-SV increased DCs maturation and antigen presentation of migratory DCs in the CLNs.

3.6. Intranasal immunization of Lipo-SV plus Lipo-HA1 did not cause observable toxicity

To evaluate nasal mucociliary toxicity, rats were i.n. administrated with Lipo-SV combined with Lipo-HA1. The scanning electron microscopic images showed that the mucosal cilia were dense and intact after i.n. immunization of Lipo-SV plus Lipo-HA1 or CTB-HA1 in comparison with PBS control (Fig. 7A). Whereas, in the group of rats treated with i.n. 1% sodium deoxycholate-HA1 (positive control), almost all the cilia were removed, indicating severe cilia toxicity. The results illustrated that i.n. Lipo-SV combined with Lipo-HA1 or CTB-HA1 did not have significant cilia toxicity.

To evaluate the safety of the Lipo-SV combined with Lipo-HA1 on major organs, we collected major organs and nasal tissues for H&E staining two weeks after the third immunization. There were no histologically significant changes in the heart, liver, spleen, kidney, and nasal mucosa of the immunized mice

treated group, the mice were i.n. immunization with Lipo-SV for 24 h, followed by i.n. immunization with Lipo-OVA-Cy5. NP, nasal passage. Blue, cell nuclei stained with DAPI. Scale bar = 10 μm. (C) Schematic illustration of Calu-3 cell monolayer cultured on the Transwell membrane for the antigen transcytosis study. (D) OVA-Cy5 fluorescence in the lower chamber at various time points following different treatments ($n = 3$). &, #, and * denote significant differences between Lipo-SV + Lipo-OVA and Lipo-OVA, Lipo-SV + Lipo-OVA and Lipo-SV + GGPP + Lipo-OVA, or Lipo-SV + Lipo-OVA and Lipo-OVA + GGPP. (E) Apparent permeability coefficient (P_{app}) calculated from the results of (D). (F, G) Immunoblotting and semi-quantitative analysis of membrane, cytosol, or total cell RAB5 (F) or RAB7B (G) levels in Calu-3 cells ($n = 3$). (H) Co-localization of OVA with lysosomes by CLSM. The cells were incubated with scrambled siRNA (Ctrl siRNA), Lipo-SV, or RAB5 siRNA for 24 h, followed by incubation with liposomes loading Cy5-labeled OVA for 3 h. The lysosomes were labeled with Lyso-tracker Red. Scale bar = 10 μm. (I) Line scan analysis along the randomly selected line in (H). Data are presented as mean ± SD. Statistical significance was assessed by one-way or two-way ANOVA with Tukey's *post hoc* test for multiple groups. $*P < 0.05$, $**P < 0.01$, $***P < 0.001$ vs. indicated, ns indicated no statistical difference between the two groups.

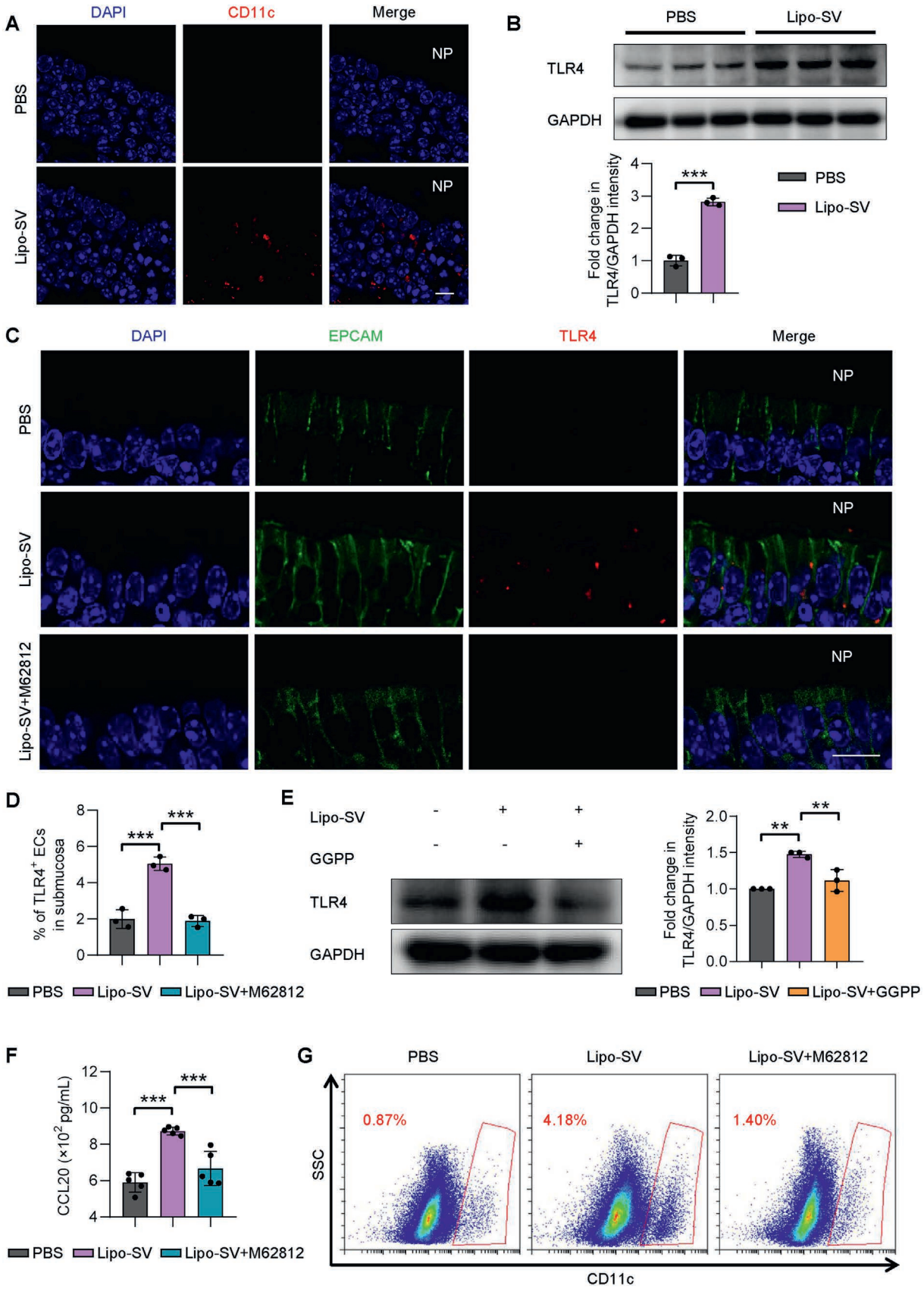

Figure 5 Lipo-SV increased DCs recruitment in the nasal mucosa through the TLR4-dependent pathway. (A) CLSM images of DCs in the lamina propria of the murine nasal cavity after i.n. administration of PBS or Lipo-SV for 24 h. DCs, $CD11c^+$ cells (Red). Blue, cell nuclei stained with DAPI. (B) Immunoblotting assays (upper) and semi-quantitative analysis (lower) of TLR4 levels in Calu-3 cells after treatment with PBS or Lipo-SV for 24 h

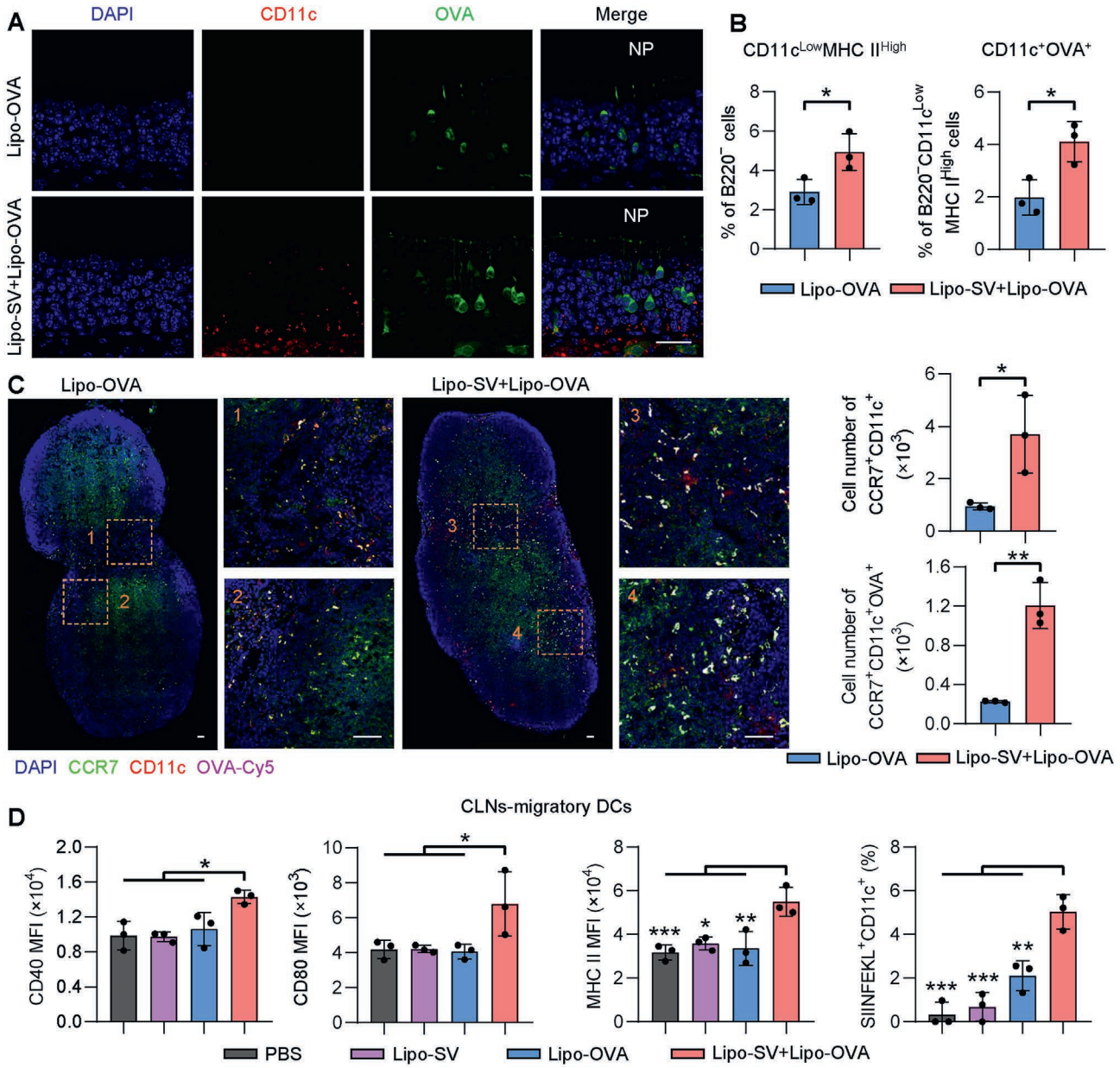

Figure 6 Lipo-SV increased DCs maturation and antigen presentation. (A) CLSM images of nasal tissues of BALB/c mice showing the submucosal recruitment of DCs and antigen uptake by DCs following i.n. administration of Lipo-OVA alone or Lipo-SV plus Lipo-OVA. Scale bar = 25 μm. (B) Mice were i.n. immunized with Lipo-OVA for 18 h, cells in the CLNs were isolated and analyzed by FCM. In the Lipo-SV-treated group, the mice were pretreated with i.n. Lipo-SV for 24 h before i.n. immunization with Lipo-OVA. Quantifications of migratory DCs ($B220^{-}CD11c^{Low}MHC\ II^{High}$) in the CLNs (left) and the OVA-loaded DCs ($B220^{-}CD11c^{Low}MHC\ II^{High}OVA^{+}$) that migrated into the CLNs (right). (C) Immunofluorescence micrograph (left) and quantifications of migratory DCs in the CLNs and OVA-loaded DCs that migrated into CLNs (right). Scale bar = 50 μm. (D) Mice were i.n. administered with PBS or Lipo-SV for 24 h, then were i.n. immunized with Lipo-OVA for 24 h. The CLNs were harvested to analyze the co-stimulators CD40, CD80, MHC-II, and SIINFEKL presentation of migratory DCs ($CCR7^{+}CD11c^{+}$). MFI = mean fluorescence intensity. Data are presented as mean ± SD ($n = 3$). Statistical significance was calculated by an unpaired two-tailed *t*-test between the two groups or by one-way ANOVA with Tukey's *post-hoc* test for multiple groups. $^{*}P < 0.05$, $^{**}P < 0.01$, $^{***}P < 0.001$ *vs*. indicated.

($n = 3$). (C, D) Fluorescence micrograph of the murine nasal cavity (C) and FCM analysis (D) of TLR4 on the nasal ECs in mice after i.n. administration of PBS, Lipo-SV or Lipo-SV plus M62812 for 24 h ($n = 3$). EPCAM, nasal epithelial cells stained with anti-EPCAM antibody. (E) Immunoblotting (left) and semi-quantitative analysis (right) of TLR4 levels in Calu-3 cells treated with PBS, Lipo-SV, or Lipo-SV co-administration of GGPP ($n = 3$). (F) The CCL20 levels in the chamber solution of Calu-3 cell monolayer after treatment with PBS, Lipo-SV, or Lipo-SV plus M62812 for 24 h, determined by ELISA ($n = 5$). (G) Representative plots of FCM analysis of nasal submucosal DCs after i.n. administration with PBS, Lipo-SV alone or Lipo-SV plus M62812 for 24 h ($n = 3$). Data are presented as mean ± SD. Statistical significance was calculated by an unpaired two-tailed *t*-test between the two groups or by One-way ANOVA with Tukey's *post-hoc* test for multiple groups. $^{*}P < 0.05$, $^{**}P < 0.01$, $^{***}P < 0.001$ *vs*. indicated.

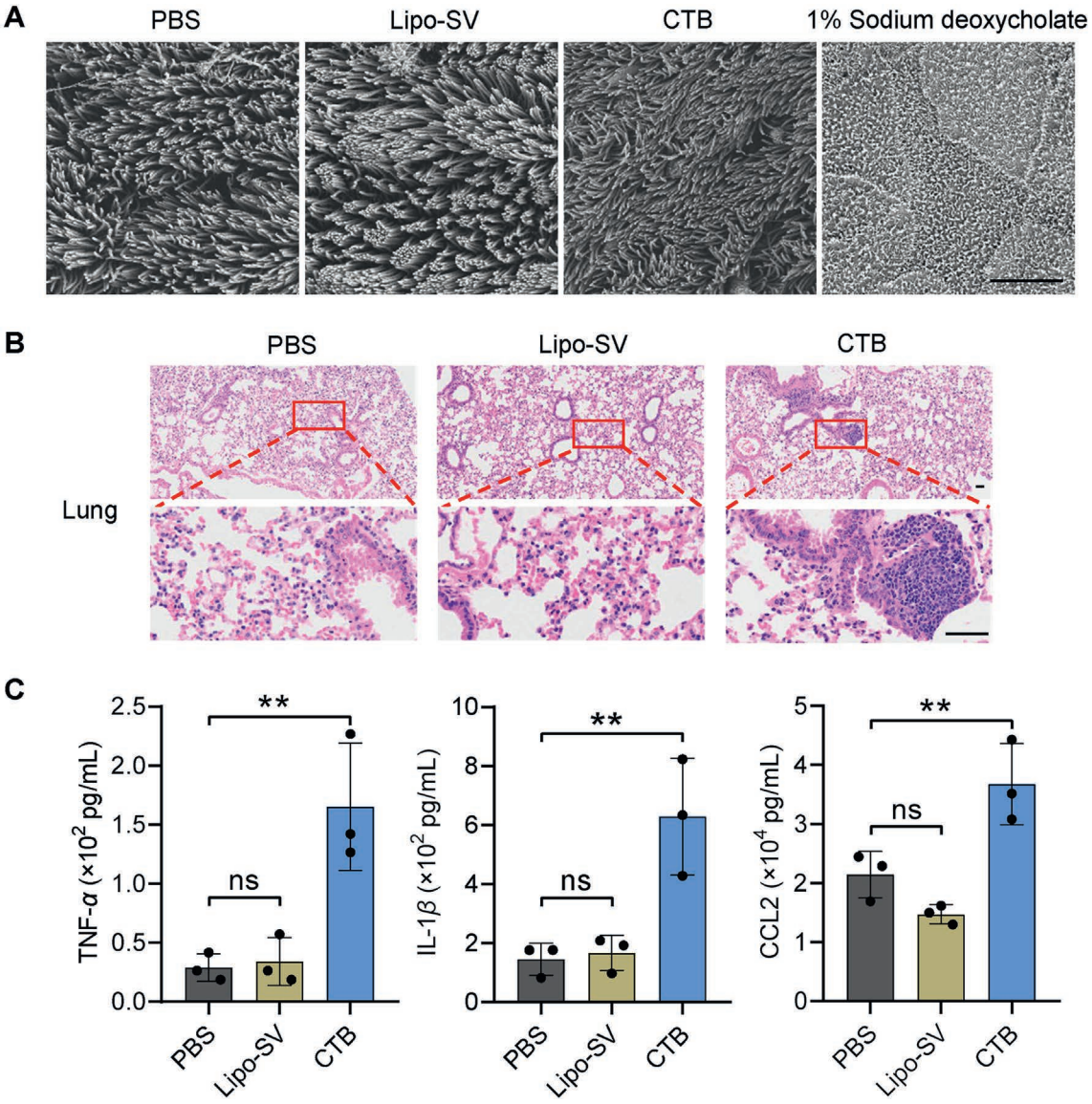

Figure 7 Lipo-SV combined with Lipo-HA1 did not cause nasal cilia toxicity or inflammation in the lung and the CNS. (A) SEM images of rat mucosa after i.n. immunization with PBS, Lipo-SV + Lipo-HA1, CTB-HA1 and 1% sodium deoxycholate-HA1 for 24 h, respectively. Scale bar = 5 μm. In Lipo-SV-treated groups, the rats were pretreated with Lipo-SV for 24 h before i.n. immunization with Lipo-HA1. (B) Histological examination of the lungs of mice at two weeks after the third immunization with different i.n. HA1 vaccines. Scale bar = 50 μm. (C) The TNF-α, IL-1β, and CCL2 levels in the CNS of mice after i.n. immunization with PBS, Lipo-SV + Lipo-HA1 or CTB-HA1 were determined by ELISA (n = 3). Data are presented as mean ± SD. Statistical significance was assessed by one-way ANOVA with Tukey's *post-hoc* test for multiple groups. $^{**}P < 0.01$, ns, no statistical difference between the two groups.

(Supporting Information Fig. S44). I.n. immunization of Lipo-SV combined with Lipo-HA1 did not lead to significant infiltration of inflammatory cells in the lung. In contrast, i.n. administration of CTB-HA1 caused substantial inflammatory cell infiltration (Fig. 7B).

The potential dissemination of mucosal adjuvants to the CNS is another safety concern[38]. To evaluate the potential toxicity of Lipo-SV combined with Lipo-HA1 vaccine to the CNS, the CSF of mice was collected at two weeks post the third immunization. The results by ELISA showed that there was no significant change in cytokines in the Lipo-SV plus Lipo-HA1 group compared with the PBS control. By contrast, i.n. immunization of CTB-HA1 led to high levels of TNF-α, IL-1β and CCL2 in CSF by 5.7-fold, 4.3-fold and 1.7-fold in comparison with the PBS group, respectively (Fig. 7C). In addition, i.n. administration of Lipo-SV had no significant effect on the hematological indexes and liver and kidney function indexes of mice (Supporting Information Fig. S45), showing the biosafety of i.n. Lipo-SV plus Lipo-HA1 *in vivo*.

4. Discussion

To date, there are six U.S. Food and Drug Administration (FDA)-approved adjuvants, including aluminum salt, MF-59, AS04, AS03, CpG1018, and Matrix-M. However, none of them are used for human mucosal vaccines. These adjuvants aim to enhance the immune response by activating innate immune cells or

recognizing pathogen-associated molecular patterns (PAMPs) *via* PRRs on APCs[39]. Since APCs play a central role in processing antigens and initiating adaptive immune responses, APCs are the common targets for the design of most adjuvants. Differently, our results demonstrate nasal ECs to be an effective target for mucosal adjuvants. The nasal mucosal adjuvant Lipo-SV facilitates i.n. subunit vaccine to elicit robust both systemic and local immune responses. The underlying mechanism involves that the i.n. Lipo-SV increase the transcytosis of antigens of nasal ECs and submucosal DCs recruitment by inhibiting the geranylgeranylation of RAB5 and/or RAB7B GTPases. Other statins or bisphosphonates as the MVA pathway inhibitors, may also have such mucosal adjuvant activity. In addition, since the Rab and Rho family members are known to regulate trafficking and cargo sorting, SV may inhibit the formation of GGPP of other small GTPases to increase the transcytosis of antigens[40,41]. Agents inhibiting small GTPases may exhibit mucosal adjuvanticity.

Our findings illustrate that Lipo-SV enhance the submucosal DCs recruitment through activating TLR4. Addition of TLR4 inhibitors causes significantly decreased CCL20 secretion and submucosal DCs recruitment (Fig. 5F and G). This result suggests that Lipo-SV may activate TLR4 in the absence of TLR4 agonists. Previous studies have reported that TLR4 can be activated by the endosomal accumulation of cholesterol in the absence of any ligand[42−44]. Other study has shown that SV increases the expression of the transcriptional factor sterol regulatory element-binding protein 2 (SREBP2)[45]. When the cells are deprived of cholesterol, SREBP2 restores cellular cholesterol, which leads to the accumulation of cholesterol[46]. Our results show that Lipo-SV treatment significantly increased free cholesterol levels in endosomes compared to the untreated control (Supporting Information Fig. S46). Therefore, we hypothesize that Lipo-SV activates TLR4 by increasing the accumulation of cholesterol in endosomes.

Currently used adjuvants such as TLR agonists, cytosolic nucleotide oligomerization domain-like receptors (NODs) agonists, and C-type lectin-like receptors agonists activate the innate immune response, resulting in inflammation and production of pyrogenic factors. These adjuvants potentially contribute to adverse effects such as fever[47,48]. Although Poly(I:C) can enhance mucosal immune responses, its clinical application is limited by poor stability and potential side effects, including the promotion of allergic and autoimmune diseases[49,50]. Lipopolysaccharide (LPS), a key component of Gram-negative bacterial cell walls, is a known TLR4 agonist. It leads to a potential risk of toxicity when intratracheal inoculation including acute lung inflammation and lung injury[51,52]. The low-toxicity TLR4 agonist monophosphoryl lipid A (MPLA), a derivative of LPS, is under investigation in both preclinical and clinical settings as a mucosal adjuvant for norovirus vaccines[53,54]. We have conducted a direct comparison of the antibody titers induced by Lipo-MPLA-RBD and Lipo-SV combined with Lipo-RBD. The results showed that Lipo-SV plus Lipo-RBD induced significantly higher level of the serum IgG1 antibody titers in comparison with Lipo-MPLA-RBD (Supporting Information Fig. S47). On the other hand, Lipo-SV independent of conventional "danger sensing" through activating PRRs do not cause infiltration of inflammatory cells in the lungs or inflammatory factors in CSF. The general side effects of statins such as hyperglycemia, proteinuria and diarrhea will be evaluated in the future study.

Currently reported mucosal adjuvants such as TLR7/8 agonists, cyclic dinucleotides (CDNs), and ISCOMs exhibit significant potential as mucosal adjuvants. Yet, they face several challenges that limit their clinical application. The inflammatory effects of TLR7/8 agonists (*e.g.*, Resiquimod) primarily result from their capacity to trigger excessive production of pro-inflammatory cytokines. Furthermore, emerging clinical evidence suggests that these agents may occasionally induce distant inflammatory mucosal reactions, highlighting concerns beyond local toxicity[55]. The *in vivo* efficacy of CDNs is limited by their physicochemical properties such as negative charges, hydrophilicity, poor cellular targeting, and membrane permeability. Besides, CDNs have the potential to induce excessive systemic inflammation due to robust cytokine release[56]. ISCOMs incorporate natural saponin Quil A, which is toxic in humans and can cause severe adverse effects such as local reactions, granulomas, and hemolysis[57]. Additionally, saponins are currently obtained through plant extraction and cannot be synthetically produced[58]. In contrast, our results demonstrate good biocompatibility of Lipo-SV following three doses of vaccination, which offers a promising alternative to these platforms.

The recruitment of T cells from the bloodstream into the lung parenchyma is a critical and well-established step in the adaptive immune response to respiratory viral infections[59,60]. Concurrently, TRMs play an indispensable role in mediating locally protective immunity against respiratory pathogens, which is essential for effective viral clearance and the prevention of severe disease progression[61]. An increase in immune cells in the lung of vaccinated mice after the H1N1 viral infection has been observed in the study (Fig. 3G and Supporting Information Figs. S21−S23). It is unknown whether these lymphocytes are lung resident or rapidly recruited to the lung upon the viral challenge. In our study, i.n. immunization with Lipo-SV combined with Lipo-HA1 established a population of $CD8^+$ TRMs in the lung, evidenced by a significant increase in the frequency of $CD8^+CD69^+CD103^+$ ($CD8^+$ TRMs) cells isolated from lung tissue at two weeks after the third immunization (Fig. 2M and Fig. S14C). In future studies, isolation and characterization of subpopulations of these cells from the lung, MLNs, and peripheral blood before and after challenge will elucidate the detailed mechanisms of the cellular immunity against virus infection provided by the vaccine.

5. Conclusions

In conclusion, we have demonstrated that Lipo-SV, as an effective and safe nasal mucosal adjuvant, enhances intranasal H1N1 influenza subunit vaccines by inducing antigen-specific systemic IgG1, mucosal IgA and IgG, CLTs, and $CD8^+$ TRMs. Compared with i.m. immunization with $Al(OH)_3$-HA1, i.n. immunization with Lipo-SV plus Lipo-HA1 induces more robust systemic and mucosal immunity, and offer better protection from the PR8 H1N1 virus in both respiratory tracts and intestines. Lipo-SV inhibits the geranylgeranylation of RAB5 and/or RAB7B GTPases in nasal ECs, enhancing antigen transcytosis and promoting submucosal DCs recruitment. Unlike CTB, Lipo-SV does not induce inflammatory cell infiltration in the lungs or significant cytokine production in the brain. Taken together, our findings reveal that nasal epithelial cells, alongside APCs, are functional targets of mucosal adjuvants, offering different strategies for mucosal vaccination.

Acknowledgments

This work was supported by the National Natural Science Foundation of China (Nos. 82471857, 22595413 and 81991493, China) and Shanghai Municipal Health Commission (2022XD045,

China). We thank the National Facility for Protein Science in Shanghai (NFPS) for the Electron Microscopy System and the Integrated Laser Microscopy System.

Author contributions

Wei Lu and Afeng Yang designed the experiment. Afeng Yang, Chen Zhang, Aihua Wu, and Jiaojiao Xu carried out experiments and performed data analysis. Xunlong Shi, Hongzheng Lin, Zhe Li, Tingting Li, and Yunlu Li participated in the experiments. Tianying Zhang and Ningshao Xia prepared the antigen. Wei Lu, Afeng Yang, Tianying Zhang, Ningshao Xia and Xunlong Shi discussed about the results. Afeng Yang wrote the manuscript. Wei Lu revised the manuscript. All of the authors have read and approved the final manuscript.

Conflicts of interest

The authors declare no conflicts of interest.

Appendix A. Supporting information

Supporting information to this article can be found online at https://doi.org/10.1016/j.apsb.2025.12.021.

References

1. Neutra MR, Kozlowski PA. Mucosal vaccines: the promise and the challenge. *Nat Rev Immunol* 2006;**6**:148−58.
2. Zheng MZM, Wakim LM. Tissue resident memory T cells in the respiratory tract. *Mucosal Immunol* 2022;**15**:379−88.
3. Mitsi E, Diniz MO, Reiné J, Collins AM, Robinson RE, Hyder-Wright A, et al. Respiratory mucosal immune memory to SARS-CoV-2 after infection and vaccination. *Nat Commun* 2023;**14**:6815.
4. Hartwell BL, Melo MB, Xiao P, Lemnios AA, Li N, Chang JYH, et al. Intranasal vaccination with lipid-conjugated immunogens promotes antigen transmucosal uptake to drive mucosal and systemic immunity. *Sci Transl Med* 2022;**14**:eabn1413.
5. Lavelle EC, Ward RW. Mucosal vaccines-fortifying the frontiers. *Nat Rev Immunol* 2022;**22**:236−50.
6. Kawai A, Tokunoh N, Kawahara E, Tamiya S, Okamura S, Ono C, et al. Intranasal immunization with an RBD-hemagglutinin fusion protein harnesses preexisting immunity to enhance antigen-specific responses. *J Clin Invest* 2023;**133**:e166827.
7. Wu L, Xu WW, Jiang HY, Yang MS, Cun DM. Respiratory delivered vaccines: current status and perspectives in rational formulation design. *Acta Pharm Sin B* 2024;**14**:5132−60.
8. Baker Jr JR, Farazuddin M, Wong PT, O'Konek JJ. The unfulfilled potential of mucosal immunization. *J Allergy Clin Immunol* 2022;**150**: 1−11.
9. Csaba N, Garcia-Fuentes M, Alonso MJ. Nanoparticles for nasal vaccination. *Adv Drug Deliv Rev* 2009;**61**:140−57.
10. Jiang YH, Lei LP, Zhao MY, Tian YX, Huang YY, Yang MH. Nanocarrier vaccines for respiratory infections. *Trends Mol Med* 2025; **31**:652−68.
11. D'Mello SR, Cruz CN, Chen ML, Kapoor M, Lee SL, Tyner KM. The evolving landscape of drug products containing nanomaterials in the United States. *Nat Nanotechnol* 2017;**12**:523−9.
12. Childers NK, Tong G, Mitchell S, Kirk K, Russell MW, Michalek SM. A controlled clinical study of the effect of nasal immunization with a *Streptococcus mutans* antigen alone or incorporated into liposomes on induction of immune responses. *Infect Immun* 1999;**67**:618−23.
13. Bechtold V, Smolen KK, Burny W, de Angelis SP, Delandre S, Essaghir A, et al. Functional and epigenetic changes in monocytes from adults immunized with an AS01-adjuvanted vaccine. *Sci Transl Med* 2024;**16**:eadl3381.
14. Coffman RL, Sher A, Seder RA. Vaccine adjuvants: putting innate immunity to work. *Immunity* 2010;**33**:492−503.
15. Li X, Xu MX, Yang JY, Zhou L, Liu L, Li M, et al. Nasal vaccination of triple-RBD scaffold protein with flagellin elicits long-term protection against SARS-CoV-2 variants including JN.1. *Signal Transduct Target Ther* 2024;**9**:114.
16. Hogenesch H. Mechanism of immunopotentiation and safety of aluminum adjuvants. *Front Immunol* 2012;**3**:406.
17. Qin T, Ma S, Miao XY, Tang Y, Huangfu D, Wang JY, et al. Mucosal vaccination for influenza protection enhanced by catalytic immune-adjuvant. *Adv Sci (Weinh)* 2020;**7**:2000771.
18. Pulendran B, Arunachalam PS, O'Hagan DT. Emerging concepts in the science of vaccine adjuvants. *Nat Rev Drug Discov* 2021;**20**: 454−75.
19. Ren HZ, Jia WC, Xie YJ, Yu MH, Chen Y. Adjuvant physiochemistry and advanced nanotechnology for vaccine development. *Chem Soc Rev* 2023;**52**:5172−254.
20. Holmgren J, Czerkinsky C. Mucosal immunity and vaccines. *Nat Med* 2005;**11**:S45−53.
21. Lycke N. Recent progress in mucosal vaccine development: potential and limitations. *Nat Rev Immunol* 2012;**12**:592−605.
22. Kim MY, Vergara E, Tran A, Paul MJ, Kwon TH, Ma JKC, et al. Marked enhancement of the immunogenicity of plant-expressed IgG-Fc fusion proteins by inclusion of cholera toxin non-toxic B subunit within the single polypeptide. *Plant Biotechnol J* 2024;**22**:1402−16.
23. Xia Y, Xie YH, Yu ZS, Xiao HY, Jiang GM, Zhou XY, et al. The mevalonate pathway is a druggable target for vaccine adjuvant discovery. *Cell* 2018;**175**:1059−73.e21.
24. Wu AH, Yang AF, Tong QL, Wei GG, Zhang SH, Yu S, et al. A rationally designed cancer vaccine based on NIR-II fluorescence image-guided light-triggered remote control of antigen cross-presentation and autophagy. *Acta Pharm Sin B* 2023;**13**:3121−36.
25. Alyami MH, Ahmad MZ, Ahmad J, Abdel-Wahab BA, Pathak K. Advances in lipid-based nanoformulations for inhaled antibiotic therapy in respiratory infections. *Drug Discov Today* 2025;**30**:104380.
26. Baumjohann D, Preite S, Reboldi A, Ronchi F, Ansel KM, Lanzavecchia A, et al. Persistent antigen and germinal center B cells sustain T follicular helper cell responses and phenotype. *Immunity* 2013;**38**:596−605.
27. Rotrosen E, Kupper TS. Assessing the generation of tissue resident memory T cells by vaccines. *Nat Rev Immunol* 2023;**23**:655−65.
28. Zhou LS, Jiao YK, Tang JY, Zhao ZZ, Zhu HY, Lu Y, et al. Ultrafiltration isolation, structure and effects on H1N1-induced acute lung injury of a heteropolysaccharide from *Houttuynia cordata*. *Int J Biol Macromol* 2022;**222**:2414−25.
29. Shi CC, Su C, Cen LF, Han L, Tang JG, Wang ZT, et al. Vunakizumab-IL22, a novel fusion protein, promotes intestinal epithelial repair and protects against gut injury induced by the influenza virus. *Biomedicines* 2023;**11**:1160.
30. Wang J, Li FQ, Wei HM, Lian ZX, Sun R, Tian ZG. Respiratory influenza virus infection induces intestinal immune injury *via* microbiota-mediated Th17 cell-dependent inflammation. *J Exp Med* 2014;**211**:2397−410.
31. Grainger CI, Greenwell LL, Lockley DJ, Martin GP, Forbes B. Culture of Calu-3 cells at the air interface provides a representative model of the airway epithelial barrier. *Pharm Res* 2006;**23**:1482−90.
32. Stentebjerg-Andersen A, Notlevsen IV, Brodin B, Nielsen CU. Calu-3 cells grown under AIC and LCC conditions: implications for dipeptide uptake and transepithelial transport of substances. *Eur J Pharm Biopharm* 2011;**78**:19−26.
33. Morad G, Carman CV, Hagedorn EJ, Perlin JR, Zon LI, Mustafaoglu N, et al. Tumor-derived extracellular vesicles breach the intact blood−brain barrier *via* transcytosis. *ACS Nano* 2019;**13**: 13853−65.
34. Qin T, Yin YY, Wang XQ, Liu HF, Lin J, Yu QH, et al. Whole inactivated avian Influenza H9N2 viruses induce nasal submucosal

dendritic cells to sample luminal viruses *via* transepithelial dendrites and trigger subsequent DC maturation. *Vaccine* 2015;**33**:1382−92.
35. Iwasaki A. Mucosal dendritic cells. *Annu Rev Immunol* 2007;**25**: 381−418.
36. Wang YZ, Chen TY, Han CF, He DH, Liu HB, An HZ, et al. Lysosome-associated small Rab GTPase Rab7b negatively regulates TLR4 signaling in macrophages by promoting lysosomal degradation of TLR4. *Blood* 2007;**110**:962−71.
37. Qin T, Yin YY, Yu QH, Huang LL, Wang XQ, Lin J, et al. CpG oligodeoxynucleotides facilitate delivery of whole inactivated H9N2 influenza virus *via* transepithelial dendrites of dendritic cells in nasal mucosa. *J Virol* 2015;**89**:5904−18.
38. Nochi T, Yuki Y, Takahashi H, Sawada S, Mejima M, Kohda T, et al. Nanogel antigenic protein-delivery system for adjuvant-free intranasal vaccines. *Nat Mater* 2010;**9**:572−8.
39. Gupta A, Rudra A, Reed K, Langer R, Anderson DG. Advanced technologies for the development of infectious disease vaccines. *Nat Rev Drug Discov* 2024;**23**:914−38.
40. Agola JO, Jim PA, Ward HH, Basuray S, Wandinger-Ness A. Rab GTPases as regulators of endocytosis, targets of disease and therapeutic opportunities. *Clin Genet* 2011;**80**:305−18.
41. Qualmann B, Mellor H. Regulation of endocytic traffic by Rho GTPases. *Biochem J* 2003;**371**:233−41.
42. Suzuki M, Sugimoto Y, Ohsaki Y, Ueno M, Kato S, Kitamura Y, et al. Endosomal accumulation of toll-like receptor 4 causes constitutive secretion of cytokines and activation of signal transducers and activators of transcription in Niemann-Pick disease type C (NPC) fibroblasts: a potential basis for glial cell activation in the NPC brain. *J Neurosci* 2007;**27**:1879−91.
43. Sun Y, Ishibashi M, Seimon T, Lee M, Sharma SM, Fitzgerald KA, et al. Free cholesterol accumulation in macrophage membranes activates toll-like receptors and p38 mitogen-activated protein kinase and induces cathepsin K. *Circ Res* 2009;**104**:455−65.
44. Azzam KM, Fessler MB. Crosstalk between reverse cholesterol transport and innate immunity. *Trends Endocrinol Metab* 2012;**23**: 169−78.
45. Jia YJ, Xu RX, Sun J, Tang Y, Li JJ. Enhanced circulating PCSK9 concentration by berberine through SREBP-2 pathway in high fat diet-fed rats. *J Transl Med* 2014;**12**:103.
46. Tomita K, Teratani T, Suzuki T, Shimizu M, Sato H, Narimatsu K, et al. Free cholesterol accumulation in hepatic stellate cells: mechanism of liver fibrosis aggravation in nonalcoholic steatohepatitis in mice. *Hepatology* 2014;**59**:154−69.
47. Nanishi E, Dowling DJ, Levy O. Toward precision adjuvants: optimizing science and safety. *Curr Opin Pediatr* 2020;**32**:125−38.
48. Rappuoli R, Alter G, Pulendran B. Transforming vaccinology. *Cell* 2024;**187**:5171−94.
49. Takaki H, Kure S, Oshiumi H, Sakoda Y, Suzuki T, Ainai A, et al. Toll-like receptor 3 in nasal $CD103^+$ dendritic cells is involved in immunoglobulin A production. *Mucosal Immunol* 2018;**11**: 82−96.
50. Ko KH, Cha SB, Lee SH, Bae HS, Ham CS, Lee MG, et al. A novel defined TLR3 agonist as an effective vaccine adjuvant. *Front Immunol* 2023;**14**:1075291.
51. Wang RH, Gan CL, Mao R, Chen Y, Yan R, Li G, et al. Rat models of postintracerebral hemorrhage pneumonia induced by nasal inoculation with *Klebsiella pneumoniae* or intratracheal inoculation with LPS. *Front Immunol* 2024;**15**:1477902.
52. Jiang YH, Qi SS, Mao CQ. Polysaccharide nanoparticles as potential immune adjuvants: mechanism and function. *Acta Pharm Sin B* 2025; **15**:1796−815.
53. Baldridge JR, Yorgensen Y, Ward JR, Ulrich JT. Monophosphoryl lipid A enhances mucosal and systemic immunity to vaccine antigens following intranasal administration. *Vaccine* 2000;**18**:2416−25.
54. Alu A, Chen L, Lei H, Wei YQ, Tian XH, Wei XW. Intranasal COVID-19 vaccines: from bench to bed. *EBioMedicine* 2022;**76**: 103841.
55. Smith WA, Siegel D, Lyon VB, Holland KE. Psoriasiform eruption and oral ulcerations as adverse effects of topical 5% imiquimod treatment in children: a report of four cases. *Pediatr Dermatol* 2013; **30**:e157−60.
56. Motwani M, Pesiridis S, Fitzgerald KA. DNA sensing by the cGAS−STING pathway in health and disease. *Nat Rev Genet* 2019; **20**:657−74.
57. Aguilar JC, Rodríguez EG. Vaccine adjuvants revisited. *Vaccine* 2007; **25**:3752−62.
58. Ontiveros-Padilla L, Bachelder EM, Ainslie KM. Microparticle and nanoparticle-based influenza vaccines. *J Control Release* 2024;**376**: 880−98.
59. Springer TA. Traffic signals for lymphocyte recirculation and leukocyte emigration: the multistep paradigm. *Cell* 1994;**76**:301−14.
60. Groom JR, Luster AD. CXCR3 ligands: redundant, collaborative and antagonistic functions. *Immunol Cell Biol* 2011;**89**:207−15.
61. Uddbäck I, Michalets SE, Saha A, Mattingly C, Kost KN, Williams ME, et al. Prevention of respiratory virus transmission by resident memory $CD8^+$ T cells. *Nature* 2024;**626**:392−400.